

# ELECTRON MICROSCOPE STUDIES OF NANOSIZE IRON PARTICLES DISPERSED OVER ALUMINA SUPPORT FILMS

*by*

**RAJEEV RANJAN**



DEPARTMENT OF MATERIALS SCIENCE

INDIAN INSTITUTE OF TECHNOLOGY KANPUR

April, 1994

TH  
MS/1994/M  
R137c

4  
N  
E

ELECTRON MICROSCOPE STUDIES OF NANOSIZE IRON PARTICLES DISPERSED  
OVER ALUMINA SUPPORT FILMS

A Thesis Submitted  
in Partial Fulfilment of the Requirements  
for the Degree of  
MASTER OF TECHNOLOGY

by

RAJEEV RANJAN

to the

DEPARTMENT OF MATERIALS SCIENCE  
INDIAN INSTITUTE OF TECHNOLOGY KANPUR

APRIL, 1994

TH  
530.41  
R 1E72

25 APR 1994

LIBRARY  
ACQUISITION

Doc. No. A. 117719

MS-1994-M-RAN-ELE

*TO MY*

*PARENTS*

## ACKNOWLEDGEMENT

With deep sense of gratitude and respect I take this opportunity to express my sincere thanks to my thesis supervisor Prof. Jitendra kumar for lending me every possible help throughout the thesis work.

I am grateful<sup>to</sup> Mr. Subhash Chand for his magnanimity, who despite of a very busy work schedule, could spare time, invaluable for me.

I am thankful to Uma Mahesh and Sanjeev Sinha for offering me invaluable time, especially during the finishing stages of the thesis work.

I am also thankful to the members of Dr. D.C.Agrawal Laboratory for their co-operation throughout my thesis work.

Finally, I thank all the staff members of A.C.M.S.

  
Rajeev Ranjan

# CONTENTS

	Page
LIST OF TABLE	i
LIST OF FIGURES	ii
ABSTRACT	
CHAPTER 1: INTRODUCTION	1
CHAPTER 2: EXPERIMENTAL DETAILS AND PROCEDURES	
2.1: Substrate preparation	7
2.2: Dispersion of Particles	9
2.3: Heat Treatment Procedure	10
2.4: Specimen Characterization	13
2.5: Particle Size Determination	15
2.6: Graphical Representation of Data	15
(a) Histogram	16
(b) Size Frequency Curve	16
(c) Cumulative Plots	17
2.7: Determination of Size Distribution Parameters	17
(a) Measure of Location	17
(b) Measure of Dispersion	19
CHAPTER 3: RESULTS AND DISCUSSION	21
3.1: Alumina Substrate	21
3.2: Emergence of Particles	21
3.3: Heat Treatment	32
(a) Effect of Hydrogen	32

	(b) Effect of Oxygen	44
	(c) Effect of Vacuum	46
3.4	General Discussion	46
CHAPTER 4:	CONCLUSIONS	53
REFERENCES		56

TABLE	TITLE	PAGE
1.1	Interfacial energy of some metal- alumina system in hydrogen.	5
3.1	Interplanar spacing and Miller indices of diffraction rings of iron particles corresponding to mass thickness of 1nm deposited over alumina support film at a substrate temperature of 500°C	26
3.2	Size distribution parameters, average surface area and dispersion parameters of iron particles of mass thicknesses 0.8nm, 1.0nm and 1.5nm deposited over alumina support film at a substrate temperature of 500°C	28
3.3	Variations in the average projected area and average height of the particles with loading and substrate temperature	31
3.4	Size distribution parameters, average surface area and dispersion parameters of iron particles corresponding to mass thickness 1nm deposited over alumina support film at substrate temperature 500°C, after heating in hydrogen at 400°C for 3h, 6h and 9h	35



3.5 Interplanar spacing and Miller indices of crystallites  
formed after heating Fe/Al<sub>2</sub>O<sub>3</sub> system of mass thickness  
1nm, in hydrogen at 500C for 7h

39

FIGURES	TITLE	PAGE
1.1	(a) Cap- shaped metal particle (m) resting on a substrate <sup>a</sup> (s), (b) cap depicted in (a) shown as part of sphere of radius r, (c) hemispherical particle with radius $\theta = 90^\circ$ and (d) cap-shaped particle with $90^\circ < \theta < 180^\circ$	
2.1	Sample holder for anodization of aluminium foil	
2.2	Schematic arrangement for anodization set up	1
2.3	Schematic diagram of the system used for heating the specimen in a controlled atmosphere of $H_2/O_2$	1
3.1	(a) and (b) Bright field transmission electron micrographs of iron particles corresponding to mass thickness 1.5nm deposited <sup>over</sup> alumina support film at substrate temperatures 400C and 500C, respectively, (c) and (d) electron diffraction pattern of regions shown in (a) and (b), respectively.	2
3.2	Bright field transmission electron micrographs of iron particles corresponding to mass thicknesses (a) 0.8nm, (b) 1.0nm and (c) 1.5nm, deposited over	2

alumina support film at substrate temperature 500°C.

- 3.3 Histograms showing size distribution of iron particles corresponding to mass thicknesses (a) 0.8nm, (b) 1.0nm and (c) 1.5nm, deposited over alumina support films at substrate temperature 500°C.
- 3.4 Normal size distribution curves of iron particles corresponding to mass thickness (a) 0.8nm, (b) 1.0nm and (c) 1.5nm, deposited over alumina support films at substrate temperature 500°C.
- 3.5 Cumulative percentage versus projected diameter of iron particles corresponding to mass thicknesses (a) 0.8nm, (b) 1.0nm and (c) 1.5nm, deposited over alumina support films at substrate temperature 500°C.
- 3.6 (a) and (b) Bright field transmission electron micrographs of crystallites after heat treatment of iron particles (mass thickness 1.0nm) in hydrogen atmosphere at 400°C for 3h and 9h respectively, (c) electron diffraction pattern of region shown in (b)
- 3.7 Histogram showing size distribution of iron particles (mass thickness 1.0nm) after heat treatment in hydrogen at 400°C for (a) 3h, (b) 6h and (c) 9h.

8	(a) Normal size distribution curves and (b) Cumulative percentage versus projected diameter plots of iron particles (mass thickness 1nm) in hydrogen atmosphere at 400C for (i)3h, (ii)6h and (iii)9h.	37
9	(a) and (b) Bright field transmission electron micrographs of crystallites after heat treatment of iron particles (mass thickness 1.0nm) in hydrogen atmosphere at 500C for 2h and 7h, respectively; (c) and (d) electron diffraction pattern of regions shown in (a) and (b), respectively.	38
10	Bright field transmission electron micrographs of crystallites after heat treatment of iron particles of mass thickness 1.5nm at (a) 400C for 3h and (b) further treatment at 500C for 5h; (c) and (d) electron diffraction patterns of regions shown in (a) and (b), respectively.	40
11	Typical transmission electron micrographs of (a) core-and-ring and (b) torus shaped particles.	42
12	Transmission electron Micrographs of same region at a tilt 0° and 6° of the specimen exhibiting torus shaped crystallites for stereoscopic vision.	43
13	(a) Bright field transmission electron micrograph of crystallites after heat treatment of iron particles.	45

(1nm mass thickness) in *oxygen* atmosphere at 400C for 4h,  
(b) electron diffraction pattern of region shown in (a),  
and (c) bright field electron micrograph of crystallites  
after heating the sample corresponding to fig.3.10(b)  
in *oxygen* at 500C for 2h.

3.14 (a) and (b) Bright field and corresponding dark field  
transmission electron micrograph after heat treatment of  
iron particles (mass thickness 0.8nm) in vacuum ( $<10^{-5}$  torr)  
at 500 for 3h; (c) electron diffraction of region shown in  
(a) with objective aperture used for recording the dark  
field image (b).

## ABSTRACT

Nanosize particles of iron are dispersed over alumina support films by vacuum deposition technique at substrate temperatures of 450 and 500°C in vacuum  $\sim 10^{-5}$  torr and studied with regard to their size distribution, shape, and crystal structure by transmission electron microscope. The aim has been to understand the behaviour of iron in finely divided state in hydrogen, vacuum and oxygen ambients. It is shown that deposits of iron corresponding to mass thickness in the range 0.8 nm to 1.5 nm yield reasonable dispersion of particles. Their nature, however, depends on the temperature of the substrate, mass of iron evaporated and the local characteristics of the support. Iron crystallites undergo a chemical change to  $\text{FeAl}_2\text{O}_4$ , displaying f.c.c structure with space group Fd3m when heated in hydrogen (99.9% purity) or vacuum ( $< 10^{-5}$  torr) at 500°C. The reaction occurs very slowly at 400°C, giving a mixture of Fe,  $\text{Fe}_2\text{O}_3$  and  $\text{FeAl}_2\text{O}_4$ . Such a composite phase is identified with core-and-ring shaped particles. However  $\text{FeAl}_2\text{O}_4$  phase is achieved at 300°C by giving heat treatment in oxygen for 45 minutes only. The lattice parameter of  $\text{FeAl}_2\text{O}_4$  crystallite formed is shown to be always greater than the reported bulk value of 8.1534 Å. The exact value, however, depends on the chemical environment in which the heat treatment is carried out. Moreover, the  $\text{FeAl}_2\text{O}_4$  formation in hydrogen or oxygen atmosphere is identified with appearance of torus shaped crystallites. Re-appearance of core-and-ring structure is also observed after heat treatment of the torus shaped particles in oxygen at 500°C for 2 hours.

## 1. INTRODUCTION

Ultra fine particles (UFP's) represent the highly dispersed state of material. They are bigger than so called atoms and yet smaller than conventional fine powders. Sometime they are termed as nano size particles as well. These particles exhibit unique structural, physical and chemical properties which originate mainly due to large surface to volume ratio. Therefore, they have found immense application in the areas such as catalysis, photography, high density recording media, heat exchangers, piezoelectric devices, etc. [1-11]. As a consequence, UFP's have been receiving considerable attention in recent years, both from fundamental and application point of view, particularly to understand the origin of their nature and their curious characteristics [12-18]. Ultra high vacuum technology, thin film physics, surface science and associated instrumentation have contributed a great deal in this direction. Of particular interest are metal of group VIII in the periodic table viz. Fe, Co, Ni, Ru, Pd, Os, Ir and Pt. Among these Pd and Pt have been studied extensively on various kind of substrates, e.g  $\text{Al}_2\text{O}_3$ ,  $\text{SiO}_2$ ,  $\text{ZrO}_2$ ,  $\text{TiO}_2$  etc. [19]. Iron being the most reactive of group VIII constitutes a good choice for investigation in the ultra fine state. The present work was therefore undertaken with the objective to form iron particles on non porous alumina support films and study their behaviour in vacuum, as well as in oxygen and hydrogen atmosphere. Two important reactions, where use of iron as a catalyst is preferred are 1) Fischer-Tropsch process of

hydrocarbon synthesis, and 2) Ammonia synthesis. A supported iron catalyst when used in the reaction  $\text{CO}/\text{H}_2$  can give almost pure methane or a mixture of saturated hydrocarbons, also alcohols aldehydes and other oxygen containing products [21,23]. Fe, Ru, and Co are the best ones for heavier hydrocarbon synthesis as they dissociate CO easily and generates a very high concentration of  $\text{CH}_x$  groups. In an another interesting observation regarding the effect of substrate, Vanice [20,22] reported that the activity of CO hydrogenation at 500°C with Fe/ $\text{Al}_2\text{O}_3$  system used as a catalyst is four order of magnitude higher in comparison to Fe/ $\text{TiO}_2$  system. The main reason of selecting iron as a catalyst in ammonia synthesis is due to the fact that iron chemisorbs ammonia without dissociating it which is not the case when Ni or Pd are used [23].

The investigators so far have dealt with the particle formation method which involves vacuum evaporation of a metal on a suitable substrate and subsequent annealing or heat treatment in hydrogen at elevated temperatures. Although the particle formation does takes place in this process, yet their purity is questionable. This argument has much relevance for metals which are very reactive like iron, palladium, nickel etc. Therefore an alternative approach [16] is adopted here, in which, the particles are formed during the deposition step itself by maintaining the substrate at elevated temperature at a working pressure of  $10^{-5}$  torr or lower. Thus the method eliminates altogether the annealing or the treatment step mentioned above and supposedly yields samples, free of gaseous contamination, for carrying out



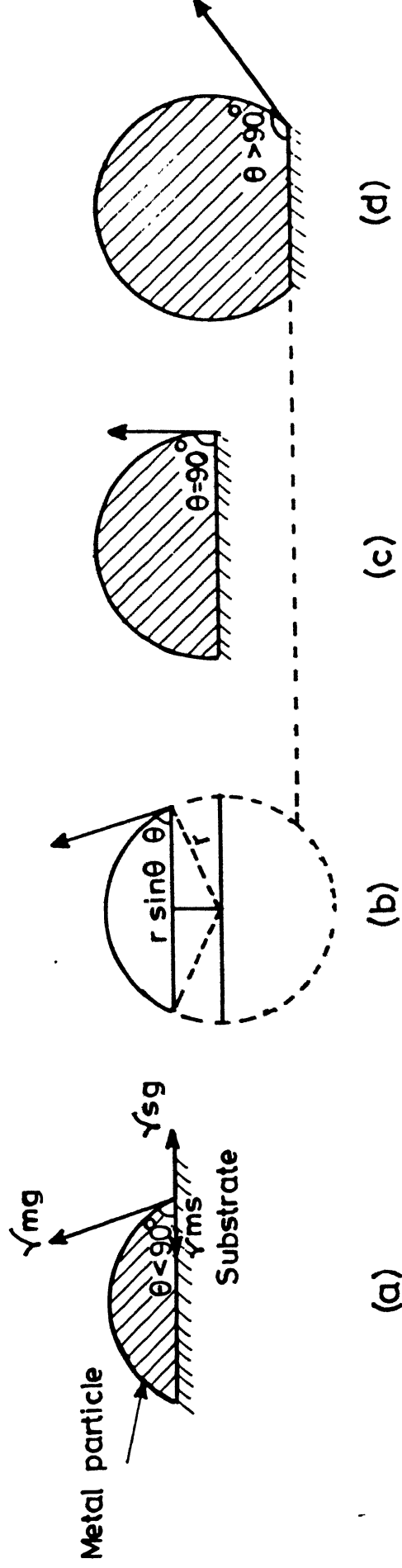


Fig. 1.1 (a) Cap-shaped metal particle (m) resting on a substrate (s),  $\gamma_{mg}$ ,  $\gamma_{ms}$  and  $\gamma_{sg}$  are metal-gas, metal-substrate and substrate-gas, interfacial energies respectively.  
 (b) Cap depicted in (a) shown as part of sphere of radius,  $r$ .  
 (c) Hemispherical particle with  $\theta = 90^\circ$   
 (d) Cap-shaped particle with  $90^\circ < \theta < 180^\circ$

meaningful studies relating to their behaviour in vacuum, oxygen and hydrogen atmospheres.

The knowledge of size, shape, and distribution of the particles is vital for understanding their overall behaviour. There are a number of methods available to-date for characterization of size, dispersion and hence the surface area of the particles. They include gas chemisorption, X-ray line broadening, small angle scattering, Mössbauer spectroscopy, extended X-ray fine structure (EXAFS), transmission electron microscopy (TEM), etc. [15, 24-33]. A brief review describing their uses and limitations has been given by Matyi, Schwartz and Bowt [34]. Of these, TEM proved to be most powerful and unique tool for characterising supported metal particles because of its usefulness in allowing resolution down upto the atomic level and simultaneously providing the crystallographic information of the material under investigation through selected area diffraction. The microstructure clearly depicts the shape of the particles along with their size distribution at a magnified scale. For this reason use is made of TEM for characterization of the fine particles.

The shape of small particles formed on a substrate by heterogeneous nucleation is determined by a parameter called contact angle  $\theta$  (fig 1.1) and associated interfacial energies. This is described better in the form of Young's equation :

$$\gamma_{mg} \cos \theta = \gamma_{sg} - \gamma_{ms}$$

TABLE 1.1: Interfacial energies of some metal-alumina systems  
in hydrogen atmosphere [35]

System	$\gamma_{sg}$ (ergs/cm <sup>2</sup> )	$\gamma_{mg}$ (ergs/cm <sup>2</sup> )	$\gamma_{ms}$ (ergs/cm <sup>2</sup> )	Temperature (°C)
Au-Al <sub>2</sub> O <sub>3</sub>	995	1260	1725	1000
Ag-Al <sub>2</sub> O <sub>3</sub>	1025	1040	1630	700
Cu-Al <sub>2</sub> O <sub>3</sub>	1010	1390	1925	850
Ni-Al <sub>2</sub> O <sub>3</sub>	995	1790	2140	1000
rFe-Al <sub>2</sub> O <sub>3</sub>	995	1870	2065	1000

where  $\gamma_{mg}$ ,  $\gamma_{sg}$  and  $\gamma_{ms}$  are metal-gas, substrate-gas and metal-substrate interfacial energies, respectively.

It is now possible to classify substrate particle configuration into four types on the basis of the values of the quantity  $\gamma_{sg} - \gamma_{ms}$ , which is the difference between the substrate-gas and substrate - metal interfacial energies, and determine the extent to which the particle is able to wet the substrate. Thus, if  $\gamma_{sg} > \gamma_{ms}$ ,  $\cos\theta$  takes a positive value such that  $\theta$  lies between  $0^\circ$  and  $90^\circ$  and particle is said to partially wet the substrate. Similarly when  $\gamma_{sg} < \gamma_{ms}$ ,  $\cos\theta$  is negative and  $\theta$  lies between  $90^\circ$  and  $180^\circ$ , again the particle partially wets the substrate with the exception that when  $\theta = 180^\circ$ , it does not wet the substrate at all. This situation of "no wetting" prevails in cases where  $\gamma_{ms} - \gamma_{sg} = \gamma_{mg}$ . Lastly, if  $\gamma_{sg} - \gamma_{ms} = \gamma_{mg}$ ,  $\theta$  is zero which amounts to complete wetting of the substrate. Obviously, these considerations can be utilized to determine the equilibrium shape of particles. The interfacial energies of some metal-alumina systems, in hydrogen atmosphere, as calculated by R.M.Pillar [35] are summarized in Table 1.1. For  $\gamma$ -iron on alumina support, we get the value of contact angle around  $150^\circ$  at a temperature of  $1000^\circ\text{C}$ . In reality, however, all kinds of particle shapes are observed based on minimum energy considerations under the influence of the nature of the substrate. For example raft like particles of iron, nickel and platinum supported on titania have been observed [36,38].

## 2. EXPERIMENTAL DETAILS AND PROCEDURES

In this chapter, initially the method used for preparation of iron particles on alumina substrate is described. Subsequently, the details of heat treatment imparted to the samples are given. Finally, a brief discussion on particle size determination and various methods of graphical representation is presented.

### 2.1 SUBSTRATE PREPARATION :

Thin films of alumina used for support of the iron particles were prepared by anodisation method. For this commercial grade aluminium foil of 0.025 mm thickness was cut into small pieces of size nearly 40mm × 15mm. They were subsequently polished chemically for about 2minutes in a solution (80ml ortho-phosphoric acid + 4ml nitric acid + 16 ml distilled water) at 80°C, washed thoroughly and dried. Finally one piece of foil was mounted on the sample holder made of perspex with the backing of thick alumina foil. This assembly [Fig2.1] served as anode and was placed in a cell containing 3 wt. % tartaric acid solution in distilled water (  $\text{PH} \sim 5.5$  adjusted with  $\text{NH}_4\text{OH}$  ) as electrolyte [39,40]. A stainless steel plate of size 100mm × 42mm × 2mm placed opposite to the sample holder was made the cathode. Thus, two circular areas (diameter  $\sim 13$  mm ) of the foil were exposed to the electrolyte for anodisation. The electrodes were connected to

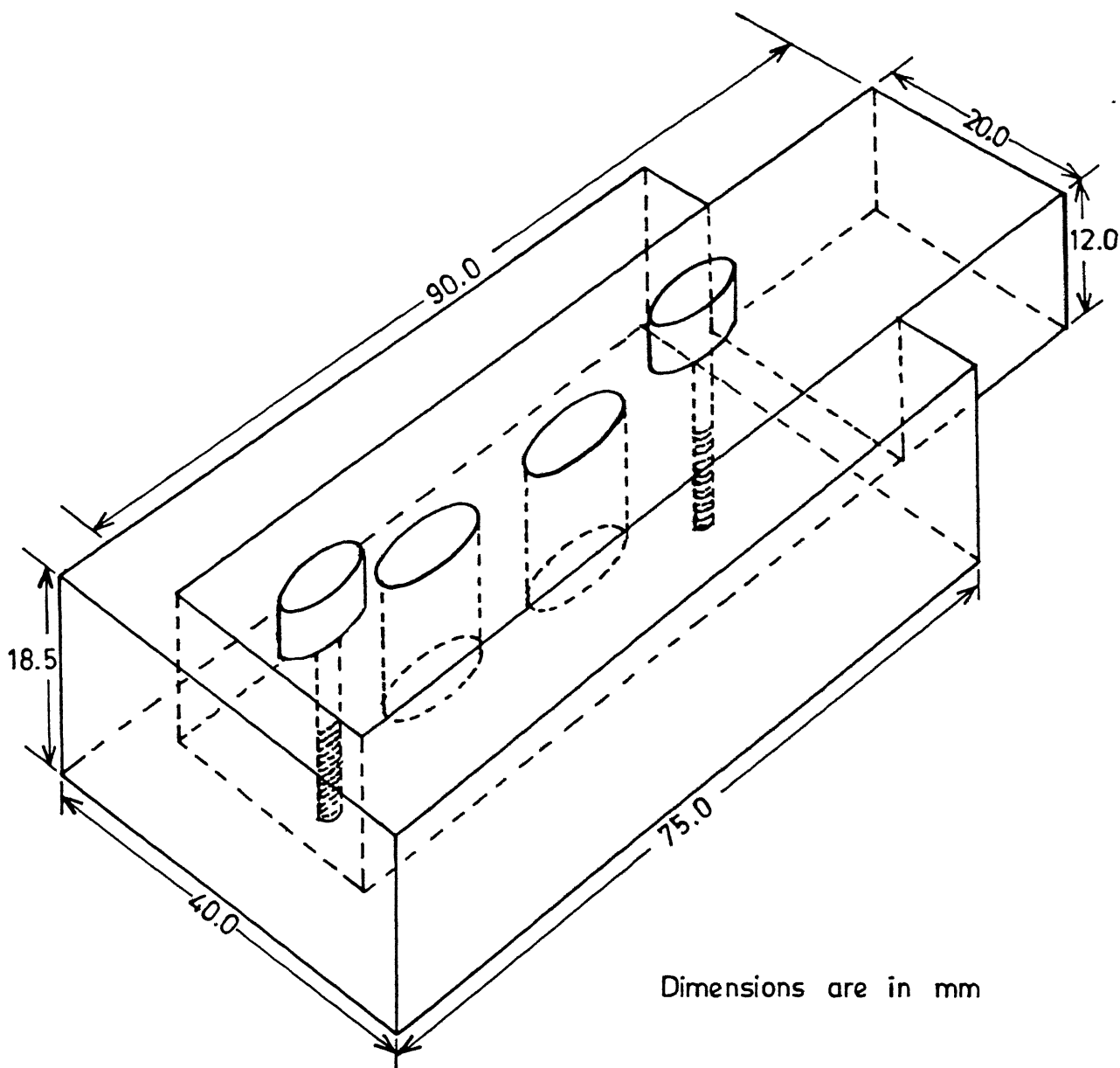


Fig. 2.1 Sample holder for anodization of aluminum foil.

a constant current power supply (CVCC, 0-30V, 0-1A) [Fig2.2]. Anodisation was carried out at 10V for one minute. The current was found to decrease sharply during the process. In this way, anodisation occurred upto a certain depth of the aluminium foil. It is known [40] that the thickness of the oxide film has a linear dependence on the applied voltage ( 1.3 nm/V ) and is practically independent of time of the anodisation upto a voltage of 20V. Therefore the thickness of the oxide film, in this case can be estimated at around 13nm. The partially anodised aluminium was then removed, washed thoroughly with distilled water and dried with an air blower in a clean atmosphere. Small pieces of the anodised foil were subsequently allowed to float, with the anodised surface up, in a solution (8g mercuric chloride + 2 ml conc. hydrochloric acid + 24 ml distilled water ) at 50°C for amalgamation. This led to the controlled dissolution of the unoxidised aluminium leaving the oxide film on the surface of the solution. The oxide film was then shifted in succession to various beakers containing distilled water to ensure thorough cleaning. Finally the alumina film was picked up on the microscopic gold grids (200 mesh, 3.05mm diameter) and allowed to dry. The resulting alumina film was non porous, quite stable and amorphous in nature.

## 2.2 DISPERSION OF IRON PARTICLES :

Iron films of average mass thickness 5 - 15 Å were deposited on alumina support by thermal evaporation in vacuum  $\sim 10^{-5}$  torr

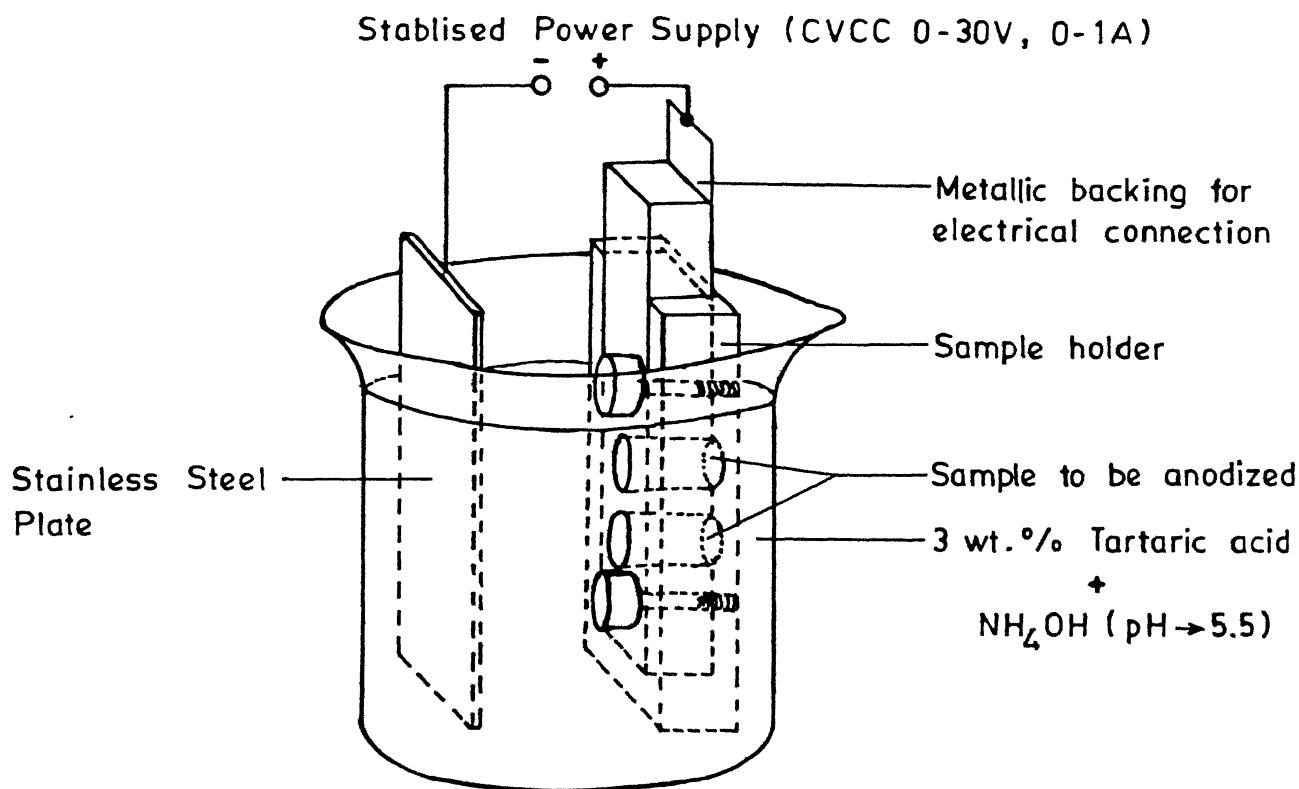


Fig.2.2 Schematic arrangement of anodization setup.



while maintaining the substrate temperature between 200 - 500°C. For this, a HINDHIVAC vacuum coating unit model 12A4D was employed. Also a small specimen heating holder comprising of tantalum sheet was fabricated which had the arrangement for placing the alumina supported grids and a chromel - alumel thermocouple. The substrate temperature was monitored by Indotherm Proportional controller 400D to a precision of  $\pm 1^\circ\text{C}$ . Mass thickness ( $t$ ) of the deposited film was determined by the amount of iron using the relation

$$M = 2\pi R^2 \rho t$$

where  $M$  (g) is the mass taken for evaporation,  $\rho$  ( $\text{g cm}^{-3}$ ) is the density of iron and  $R$  (cm) represents the distance between the evaporation source (tungsten boat) and the substrate. A known amount of iron corresponding to mass thickness 0.8, 0.9, 1.0 or 1.5nm was placed in a cleaned tungsten boat and its distance from the alumina supported grids was adjusted suitably in the working chamber. After attaining the desired vacuum, substrate was heated to remove the adsorbed gases and then set to the given temperature. Low voltage high amperage current was then passed through the tungsten boat to evaporate iron for deposition on the heated alumina substrate. The electric supply to the boat was thereafter cut-off. Also, the substrate heating was gradually lowered and finally samples were allowed to cool with vacuum pump continuously running for nearly an hour. The samples were then taken out and stored in a vacuum desiccator.

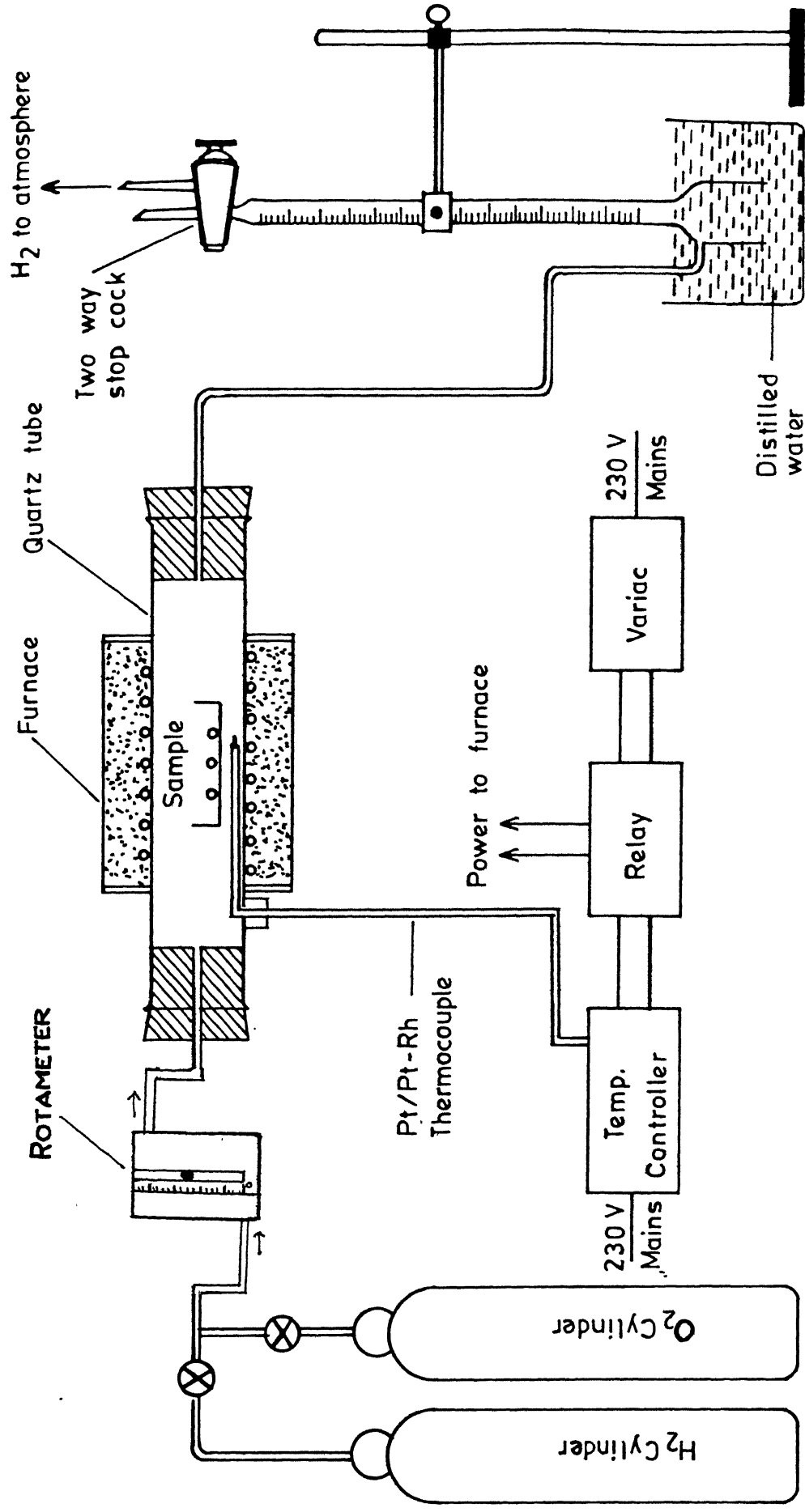


Fig.2.3 Schematic diagram of the system used for heating the specimen in a controlled atmosphere of  $H_2 / O_2$  .

### 2.3 HEAT TREATMENT PROCEDURE :

The dispersed iron particles on alumina support were heat treated in vacuum, oxygen and hydrogen at elevated temperatures (300-500°C). The heat treatment was carried out in a tubular furnace having a pre-cleaned quartz tube of 1.8 cm diameter. The samples kept in a ceramic boat of size 60mm × 10mm were introduced in the quartz tube from one end along with a K-type thermocouple. Indotherm proportional controller model 400-D was used to monitor the temperature with an accuracy of  $\pm 1^\circ\text{C}$ . The schematic picture of the heat treatment set up is given in fig 2.3. Each time the quartz tube was flushed with the respective gas to remove the contaminants present. The gas flow was then fixed at 60-70 ml per minute using the respective gas rotameter and the sample introduced in the furnace when its temperature reached the desired value. After the heat treatment for a given period, furnace power supply was cut-off. The gas flow was, however, maintained till the furnace cooled to room temperature. The samples were then taken out and stored in a vacuum desiccator. Hydrogen and oxygen used were of standard grades (99.9 % purity).

### 2.4 SPECIMEN CHARACTERISATION :

A JOEL JEM 2000 FX Mark-II transmission electron microscope (TEM) was employed to obtain information regarding the microstructure and structural crystallography of the dispersed iron particles on alumina substrates before and after subjecting

to heat treatment. The instrument was operated at 120KV. It was duly aligned each time and set for highest resolving power before observations. Moreover the illumination was always kept low to minimise contamination and other effects that usually result due to electron beam heating of the specimen. The images and the selected area diffraction (SAD) patterns were recorded on 35mm Eastman Kodak fine grain positive release film (5302). Efforts were made all along to record the high quality electron micrographs and diffraction patterns. Precise quantitative measurements right upto the resolution limit and interpretation of images and selected area diffraction patterns with possible correlation require a fairly rigorous calibration of the instrument in terms of magnification and camera constant. Magnification calibration was performed in the usual way [17,41] with a silicon monoxide ruled grating having 2160 lines per mm. Great care was taken in determining the higher magnifications in particular. Also the pictures were taken at same magnification so that comparison of the microstructures before and after the heat treatments becomes some what easier and meaningful. Evaporated iron film ( $100\text{\AA}$ ) and gold film on alumina coated grids were taken as a standard for determining the camera constant. At the time of recording SAD patterns, currents in all the lenses were noted and their variations taken into account in finding out the camera constant and, in turn, the precise values of the interplanar spacings.

## 2.5 PARTICLE SIZE DETERMINATION :

The samples were examined and micrographs recorded at suitable magnifications before and after each heat treatment. The pictures were subsequently enlarged for photographic reproduction. Electron microscopic images are nothing but planar projections of three dimensional objects. There are various methods available to date for deducing the particle size from these projections [34,42]. In the present case, projected diameters of the particles were measured on the negative itself covering different regions of a very large area and averaged. For this a computerised image analyser, model A.S.M.68K was employed. Surface average diameter, a parameter relevant to catalysis was determined by using the relation [34]

$$d_s = \frac{\sum n_i d_i^{+3}}{\sum n_i d_i^{+2}}$$

where  $n_i$  is the number of particles which have diameters between  $d_i$  and  $d_i + \Delta d_i$ , and  $d_i^+ = d_i + \Delta d_i/2$ . the values of  $d_s$  have been used to determine the surface area "S" of the particles from the expression,

$$S = \frac{6}{\rho d_s} \times 10^3 \text{ m}^2/\text{g}$$

where  $\rho(\text{g/cm}^3)$  is the material density of the particles and  $d_s$  is the surface average diameter in nm.

## 2.6 GRAPHICAL REPRESENTATION OF DATA :

Measurement data of the particle diameters can be best

represented in a graphical form [37]. It gives concise picture and allows clear visualisation of the mean value and its location. Also it ascertains the deviations and skewness of the measurements with respect to the mean value. Such a representation is useful for comparison of the data obtained from various samples and deducing the mathematical parameters defining the trend of particle distribution. There are a number of methods available for preparing the data in the graphical form. Some relevant ones are described below.

#### (a) Histogram

A histogram is a plot of the frequency of occurrence of particles as a function of a chosen size interval. It is useful for illustrating any particular frequency distribution. The ordinate may also represent weight, surface area or any other relevant parameter in specified size interval. The abscissa shows the size of the particles.

#### (b) Size frequency curve

This curve is limiting form of histogram and can be produced by simply reducing the size intervals to a minimum or else by plotting the frequency of occurrence of particles as a function of particle size. Sometimes, curve is drawn by joining the mid points of the size intervals on top of the bars. Frequency curves can be of bell, U, skew or J shape. It enables critical examination of size distributions and allows comparison of data precisely.

### (c) Cumulative plot

This is a plot of cumulative percentage of particles (0-100) versus size. Such a distribution can also be extended to other parameters like - total surface area, external surface, weight, etc. These plots provide a simple and quick way of determining the percentage, quartiles and the medians.

## 2.7 DETERMINATION OF SIZE DISTRIBUTION PARAMETERS :

Once the measurement data is tabulated and salient features displayed graphically, a number of distributed parameters can be deduced, a brief description of which now follows:

### (a) Measures of location

The purpose is to get average value of the distribution which usually lies in the central part of the curve. Various measures that are commonly employed to determine the central tendency include arithmetic, geometric and harmonic means, median and mode.

(1) *Arithmetic mean* ( $\bar{x}$ ) - It is observed for a set of observations  $X_i$  by adding together all the values of  $X_i$  and dividing by the number of observations. If  $f_i$  is the frequency of occurrence of  $X_i$

$$\text{then, } m = \frac{\sum f_i X_i}{\sum f_i}$$

This average is least affected by fluctuations of sampling and hence termed as the stable average .

(II) *Geometric mean (G)* - It is defined for a set of observations  $X_i$  as

$$G = (X_1^{f_1} \cdot X_2^{f_2} \cdot X_3^{f_3} \cdot \dots \cdot X_i^{f_i})^{1/N}$$

where  $N = \sum f_i$  is the total number of observations.

$$\text{or } \ln G = \frac{\sum f_i \ln X_i}{\sum f_i}$$

It means that natural logarithm of  $G$  is nothing but the arithmetic mean of the logarithms of the observed values. Geometric mean gives a useful description in situations where differences between the frequencies are large.

(III) *Harmonic mean (H)* - This is defined as inverse of the arithmetic mean of the reciprocals of the observed values. Thus the harmonic mean of observed values  $X_i$  with frequency  $f_i$  can be written as

$$H = \frac{\sum f_i}{\sum (f_i / x_i)}$$

This finds relevance when measurements are used to determine the number of particles per unit volume.

(IV) *Median* - It is that value of  $X$  which divides the number of



observations into two equal parts, i.e, half of the observations have values greater than  $X$  while the other half corresponds to values smaller than  $X$ . Median can be found easily from cumulative curve. This parameter is not affected by spread in extreme values and is used for visualising the data qualitatively.

(V) *Mode* - This is the most frequent value encountered in a set of observations and so corresponds to the peak of the frequency curves.

#### (b) Measures of dispersions [44,45]

After the centre of frequency distribution has been located, one can find out parameters which indicate the width of the frequency curve, i.e., how closely probabilities cluster about the mean. This is better understood in terms of moments, which can be taken around any particular location. For example,  $K^{th}$  moment around the origin can be defined as

$$M_k = \frac{\sum X_i^k f_i}{\sum f_i}$$

Therefore first moment around origin

$$M_1 = \frac{\sum X_i f_i}{\sum f_i}$$

which is nothing but arithmetic mean itself. Similarly  $K^{th}$  moment around the arithmetic mean

$$M_k' = \frac{\sum (X_i - m)^k f_i}{\sum f_i}$$

Now, first moment around the arithmetic mean is an average value of the deviation  $(X_i - m)$  of the variable  $X_i$  from its mean value and thus measures the degree of dispersion. This can however be negative also. Second moment around arithmetic mean is nothing but the variance (V) or square of the standard variation ( $\sigma$ ). This is most commonly accepted measure of dispersion of the frequency distribution and is given by

$$M_2 = V = \sigma^2 = \frac{\sum (X_i - m)^2 f_i}{\sum f_i}$$

$(X_i - m)^2$  is positive for all values of  $X_i$ . Third moment around the arithmetic mean is

$$M_3 = \frac{\sum (X_i - m)^3 f_i}{\sum f_i}$$

This measures the symmetry of the distribution, e.g., for a perfectly symmetrical distribution around the mean value,  $M_3 = 0$ . Depending upon the third moment which can be positive or negative, one gets a symmetric picture of the distribution and location of tail on one or the other side of the peak. This is defined by yet another parameter as skewness =  $M_3/\sigma^3$ .

Generally, when skewness is positive, arithmetic mean is greater than mode and median both. Also, the tail is towards higher values of  $X$  in the size distribution (i.e. right of the peak).

### 3. RESULTS AND DISCUSSION

#### 3.1 ALUMINA SUBSTRATE:

Alumina support films, prepared in the manner described in chapter 2, showed broad and diffuse haloes, characteristics of amorphous material, in their diffraction patterns. Moreover, they were continuous, electron beam transparent and possessed microstructure that did not cause any interference in observing the particles dispersed over them. The films were found to be quite stable and showed no significant rupture as a result of irradiation with electron beam during observation and after heat treatment even at elevated temperatures.

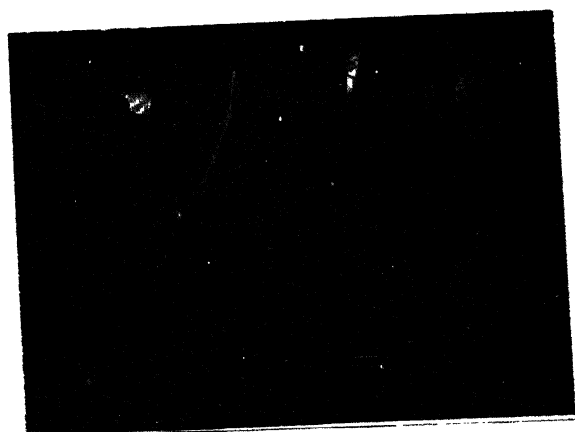
#### 3.2 EMERGENCE OF PARTICLES:

CENTRAL LIBRARY  
1 JAN 68  
Acc. No. A. 117718

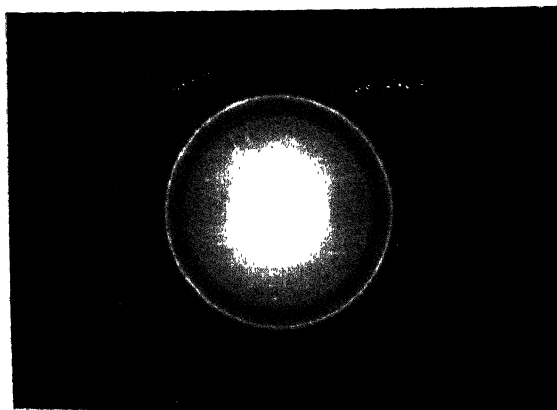
The dispersion of iron particles over alumina support films were made by a technique [15-18] in which substrate was heated and held at a fixed elevated temperature during metal evaporation under vacuum ( $<10^{-5}$  torr). This technique is actually derived from (1) conventional method of epitaxial growth of solid films over crystalline substrate and (11) procedure actually adopted for decorating the cleavage steps in alkali halides.

In the beginning vacuum deposition of iron on alumina was carried out at different substrate temperatures and for various mass thicknesses, mainly, to determine the optimum conditions for good dispersion of particles. For iron, it was found that well

separated particles start forming at a substrate temperature around 450°C. Incidentally this threshold temperature of particles emergence is much higher than those reported for the formation of gold and nickel particles (i.e., 125°C and 300°C, respectively) [17,18]. This finding indicates that iron spreads to a greater extent on alumina support than both gold and nickel. Representative transmission electron micrographs and corresponding diffraction patterns of iron films of mass thickness 1.5nm deposited over alumina at substrate temperatures of 400°C and 450°C are shown in fig 3.1. The diffuse diffraction rings in fig 3.1c clearly reveal that proper crystallinity is not achieved at substrate temperature 400°C. The corresponding micrograph also shows nearly continuous film structure of fine grain size. Fig 3.1c however indicates the emergence of platelet shaped particles with smooth edges at 450°C. The corresponding diffraction rings [fig3.1d] are quite sharp. Indexing of pattern (Table 3.1) reveals the existence of a body centered cubic phase with lattice parameter  $2.86 \pm 0.04 \text{ \AA}$  matching very well, within the experimental error, with the bulk value of iron ( $2.866 \text{ \AA}$ ) [46]. Iron particles formed at substrate temperature 500°C show <sup>[Fig 3.2]</sup> better three dimensional character (viz., depict shrinkages) than those resulted at 450°C. The above description holds good for cases of mass thicknesses 1.0nm and 0.8nm as well. Due to better dispersion of particles at substrate temperature 500°C, deposition of the iron films were carried out later at this temperature only for further study under different ambients. The variation of particle size distribution parameters with loading at substrate temperature 500°C is summarized in Table 3.2. Figs 3.3-3.5 show graphically the size



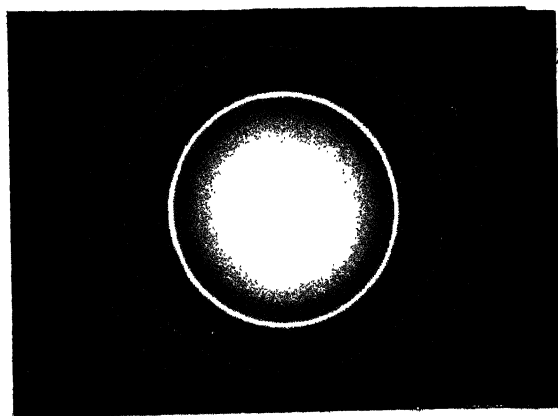
(a)



(c)



(b)



(d)


200nm  


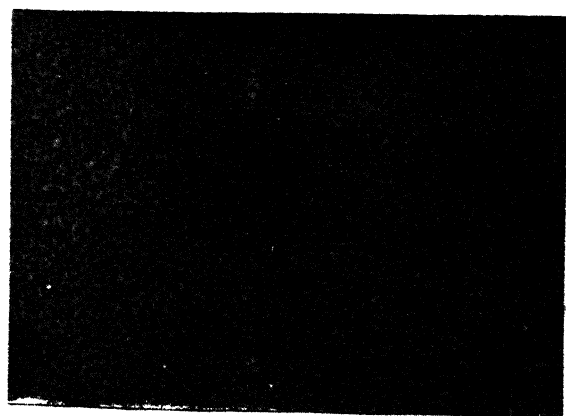
Fig.3.1: (a) and (b) Bright field transmission electron micrographs of iron particles corresponding to mass thickness 1.5nm deposited on alumina support film at substrate temperatures 400°C and 500°C respectively, (c) and (d) electron diffraction pattern of regions shown in (a) and (b), respectively.

Table 3.1: Interplanar spacing and Miller indices of diffraction rings of iron particles corresponding to mass thicknesses of 1.0nm deposited over alumina at substrate 500 C.

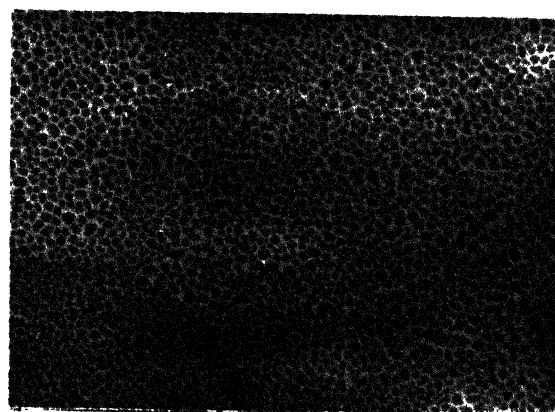
Ring No.	Observed data		Miller indices (hkl)	Known data for iron [46]	
	$d_{hkl}$ in Å ( $\pm 0.04\text{Å}$ )	Relative intensity		$d_{hkl}$ (Å)	Relative intensity
1	2.02	VS	110	2.0268	100
2	1.44	S(-)	200	1.4332	20
3	1.17	S	211	1.1702	30
4	1.02	W	220	1.0134	10
5	0.91	W	310	0.9064	12
6	0.83	VW	222	0.8275	6
7	0.77	W	321	0.7660	-

Where, V - Very, S - Strong, and W - Weak

Lattice parameter =  $2.86 \pm 0.04 \text{Å}$



(a)



(b)



(c)

200nm

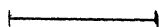


Fig.3.2: Bright field transmission electron micrographs of particles corresponding to mass thicknesses (a)0.8nm, (b)1.0nm (c)1.5nm, deposited over alumina support film at substrate temperature 500°C.

Table 3.2: Size distribution parameters, average surface area and dispersion parameters of iron particles of mass thicknesses 0.8nm, 1.0nm and 1.5nm deposited over alumina at a substrate temperature of 500 C.

Parameters	Mass thickness (nm )		
	0.8	1.0	1.5
1 Number of particles counted	1560	1560	1560
2 Distribution of peak particles ( % )	43.8	43.7	31.7
Size range (nm)	6.7 - 8.9	8.9 -13.4	13.4 - 17.8
3 Median (nm)	6.2	6.8	15.6
4 Average particle size $d_s$ (nm)	8.6	11.9	21.4
5 Average surface area S ( $m^2/g$ )	89.1	64.3	35.6
6 Particle size :			
Arithmetic mean (nm)	7.5	9.7	17.8
Geometric mean (nm)	7.2	9.1	17.1
Harmonic mean (nm)	6.9	8.4	16.2
Area length (nm)	8.0	10.8	19.7
Volume weighted (nm)	9.1	12.9	23.2
Standard deviation (nm )	1.9	3.0	5.4
Third moment ( $nm^3$ )	3.9	1.5	116.3
Skewness	0.6	0.1	0.7



distribution parameters via histogram, normal distribution and cumulative percentage plots. It is observed that the particle size increases with increase in loading for the substrate temperature of 500°C. Also it can be noticed that the average surface area (S) of the particles decreases by more than half for 1.5nm loading in comparison to the case of 0.8nm. A rough estimate of the particles average height was made by

$$\text{height} = \frac{(\text{Area of the selected region}) \times \text{Mass thickness}}{\sum A_i}$$

where  $A_i$  represents the projected area of the  $i^{\text{th}}$  particle and measured directly by using Leitz Image Analyzer Model ASM68K. The above relation always gives a value of height more than the chosen mass thickness as the entire substrate area is not fully covered by the particles. It is so as the mass that ought to be in between the particle contributes to the increase in the particles height. In Table 3.3 is given the average projected area of the particles and a rough estimate of the particles average height as a function of loading (mass thickness) and substrate temperature. It is seen that the ratio of average particle diameter and height for the 0.8nm mass thickness is more than twice the corresponding value for 1.5nm mass thickness film at the same substrate temperature of 500°C.

One important point that needs to be emphasized here is that the undertaken method of forming particles during the deposition process itself for behavioural study in different ambients is unique and somewhat distinctive from those of Suhumna and

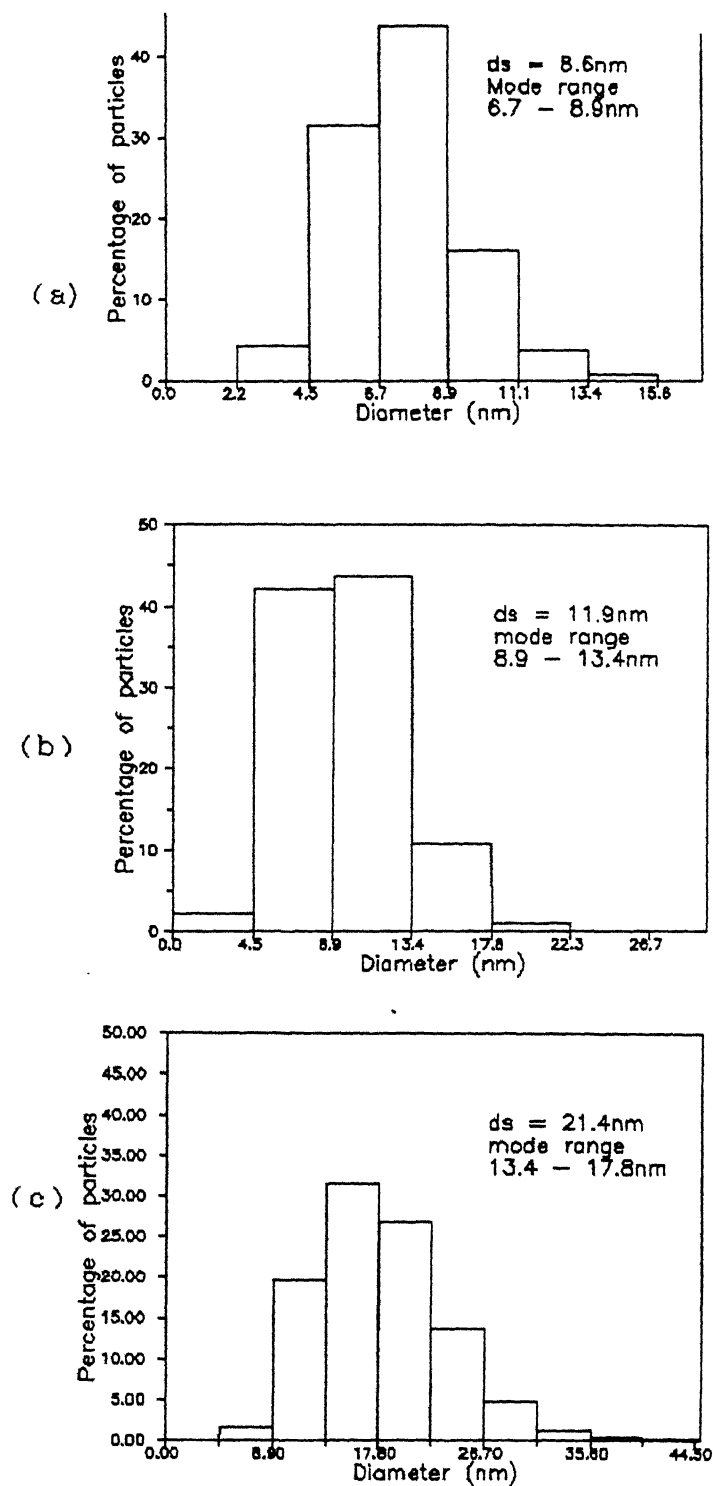


Fig.3.3: Histograms showing size distribution of iron particles corresponding to mass thicknesses (a)0.8nm, (b)1.0nm and (c)1.5nm deposited over alumina support films at substrate temperature 500°C.

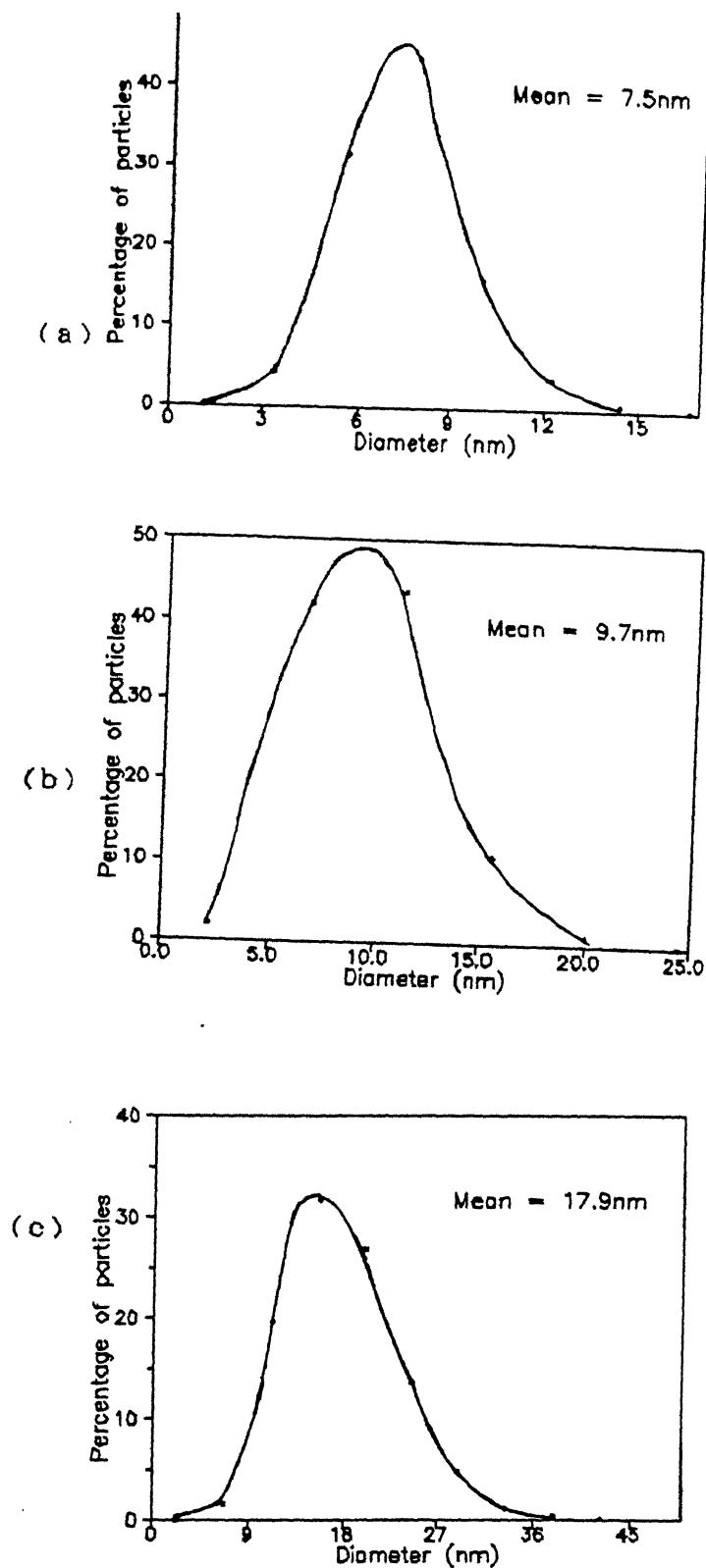


Fig.3.4: Normal size distribution curves of iron particles corresponding to mass thickness (a) 0.8nm, (b) 1.0nm and (c) 1.5nm deposited over alumina support films at substrate temperature 500°C

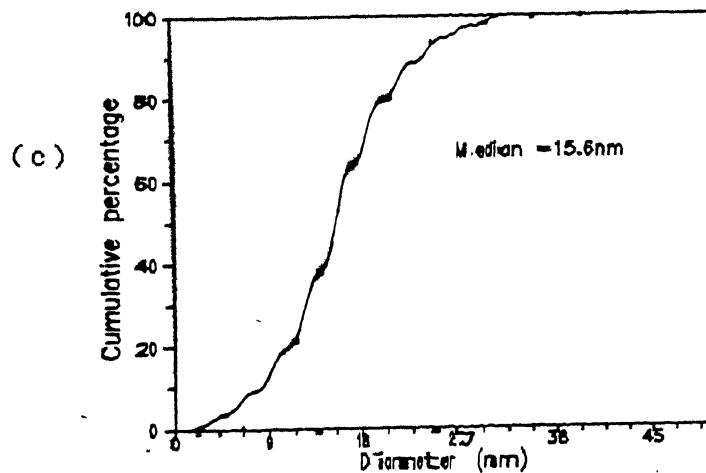
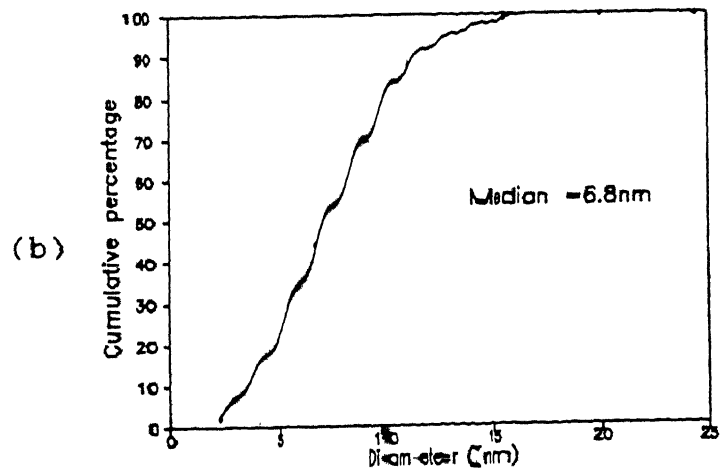
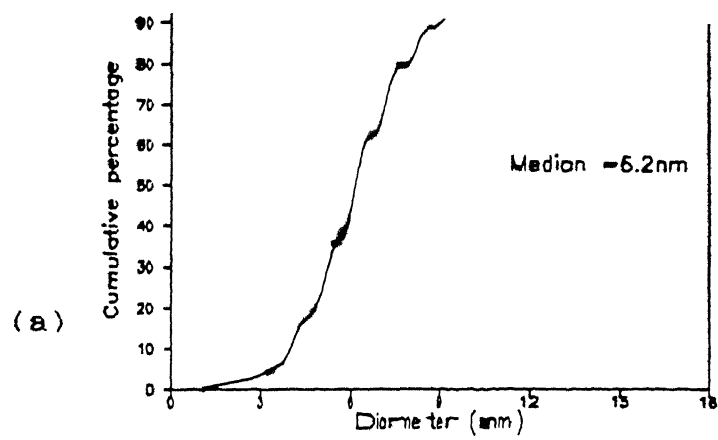


Fig.3.5: Cumulative percentage versus projected diameter of ir particles corresponding to mass thicknesses (a)0.8nm, (b)1.0nm and (c)1.5nm, deposited over alumina support films at substrate temperature 500C.

Table 3.3: Variations in average area ( $\text{nm}^2$ ) and average particle height (nm) of the particles with loading and substrate temperature.

Loading (nm)	Average projected area ( $\text{nm}^2$ )		Average height of particles (nm)	
	450C	500C	450C	500C
0.8	-	47.5	-	2.0
1.0	130.7	121.3	1.7	1.9
1.5	273.2	217.1	2.4	2.6

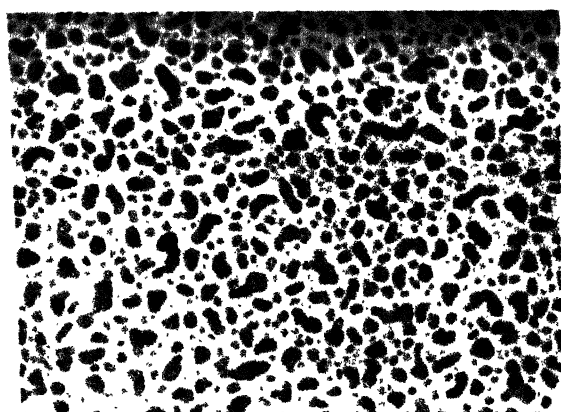
Ruckenstein [48,50], who prepared particles in the usual way by first evaporating the metal on a substrate held at room temperature and heating subsequently in hydrogen at elevated temperatures (100-800). Firstly, no distinct crystallites emerged on heating the film (mass thickness 0.6-1.2nm) in hydrogen at 300C for 12hrs. Secondly, at 400C the resulting particles were not of iron. So, the present method assumes significance in the sense that it is able to (i) yield pure iron particles during the deposition process itself and (ii) eliminate the heat treatment step (in hydrogen) altogether.

### 3.3 HEAT TREATMENT:

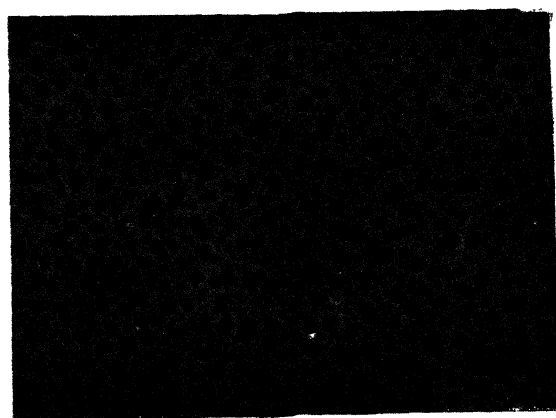
Iron samples of mass thicknesses 0.8nm, 1nm, and 1.5nm, prepared at substrate temperature 500C, were heat treated in hydrogen, oxygen and vacuum in temperature range 300-500C for different lengths of time and examined in a TEM for possible changes in morphology, phases, etc.

#### (a) Effect of Hydrogen

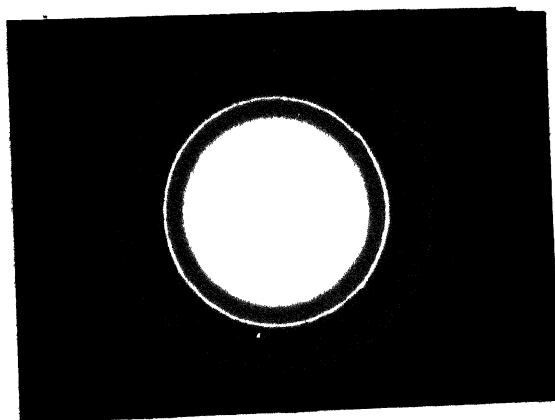
Some very large irregular shaped island type particles emerged after heating the samples in hydrogen at 400C for 3hours. The microstructure also shows fairly good fraction of particles having sizes even smaller than the original one [Fig.3.6a]. Further, heating for another 3 hours duration resulted in somewhat uniform distribution of particles with big irregular shaped particles turning relatively smaller and assuming smooth boundaries and



(a)



(b)



(c)

200nm

Fig.3.6: (a) and (b) Bright field transmission electron micrographs of iron particles (mass thickness 1.0nm) in hydrogen atmosphere at 400°C for 3h and 9h, respectively, (c) electron diffraction pattern of region shown in (b)

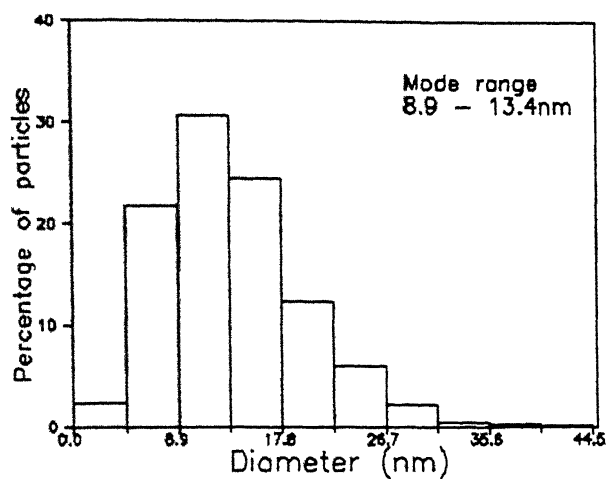
platelet character. Longer heat treatment (e.g., 9 hours) leads to an interesting phenomenon : the particles now begin to show a thin annular gap near the periphery of the particles [Fig 3.8b] . The diffraction pattern [Fig 3.6c] of such regions clearly shows that the crystallite correspond to  $\alpha$ -iron. Table 3.4 summarizes the various particle size distribution parameters determined after heat treatment in hydrogen at 400°C for 3, 6, and 9 hours. The data is represented in graphical form in Figs. 3.7 and 3.8. Another set of samples were subjected to heat treatment in hydrogen at 500°C. Here particles of platelet shape with smooth boundaries emerged just in 2 hours. <sup>[Fig 3.9a]</sup> Also the particle density decreased with the increase in heating time. The particle showed tendency of assuming round shapes. Good fraction of particles has size smaller than the original preheated situation though their number density gets slightly reduced after further heating for two hours. Increasing the heating period to 7 hours led particles to exhibit porous structure. The central portion of the particles were devoid of mass resulting in a cavity [Fig 3.9]. Moreover, each crystallites appears to be made up of large number of sub-units heaped together. Such a significant development in the particle morphology was in fact accompanied by a chemical change. The indexing [Table 3.5] of the diffraction pattern [Fig 3.9d] reveals that the crystallites correspond to a chemical composition  $\text{FeAl}_2\text{O}_4$  with face-centered cubic structure and space group  $\text{Fd}\bar{3}\text{m}$  [47]. However, the value of lattice parameter is  $8.36 \pm 0.04$  Å about 2.7% higher than the reported [47] bulk value of 8.1534 Å. In another set, one sample of mass thickness 1.5 nm was heat treated at 400°C for 3 hours in hydrogen. Fig 3.10(a-d) shows the



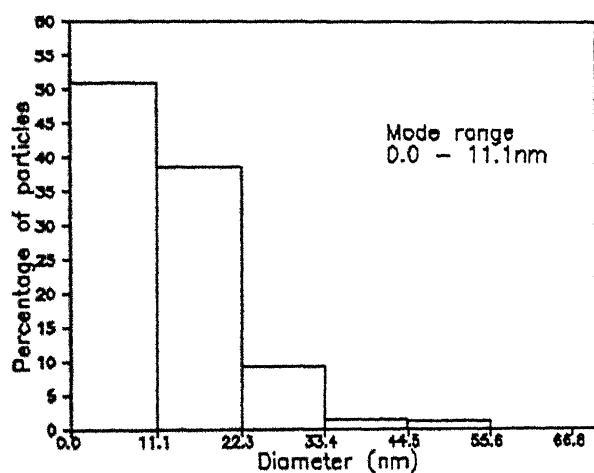
Table 3.4: Size distribution parameters, Average surface area  
Dispersion parameters of particles, corresponding to mass thickness 1nm deposited over alumina  
substrate temperature 500°C <sup>after heating</sup> in hydrogen at 400C for 3h, 6h and 9h.

Parameters	Duration of heating in hours		
	3	6	9
1.Number of particles counted	1199	1000	1230
2. Distribution of peak :			
Particles (%)	30.5	50.8	27
Size range (nm)	8.9 - 13.4	0.0 - 11.1	8.9 - 13.4
3. Median (nm)	10.5	5.5	10
4. Average particle size(nm) $d_s$	18.9	21.9	18.9
5. Average surface area "S" (m <sup>2</sup> /g)	40.3	34.8	40.3
6.Particle Size :			
Arithmetic mean (nm)	13.5	12.7	12.5
Geometric mean (nm)	12.1	10.1	10.7
Harmonic mean (nm)	10.5	8.5	8.5
Area length (nm)	16.2	17.8	15.9
Volume weighted (nm)	21.4	25.6	21.5
Standard deviation (nm)	6.0	7.1	6.4
Third moment (nm <sup>3</sup> )	182.3	443.9	194.9
Skewness	0.8	1.2	0.7

(a)



(b)



(c)

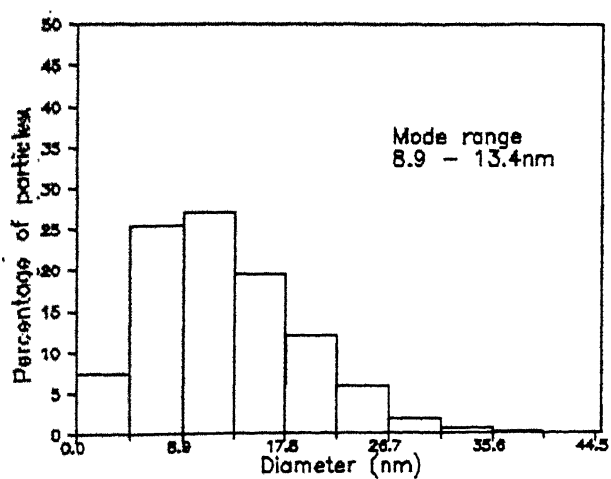


Fig.3.4: Histogram showing size distribution of iron particles (mass thickness 1.0nm) after heat treatment in hydrogen at 400C for (a)3h, (b)6h and (c)9h.

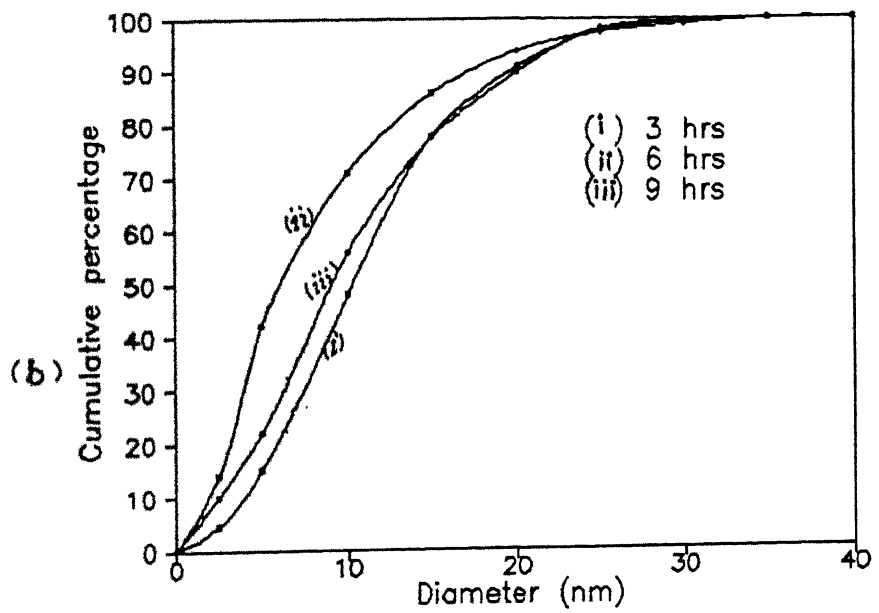
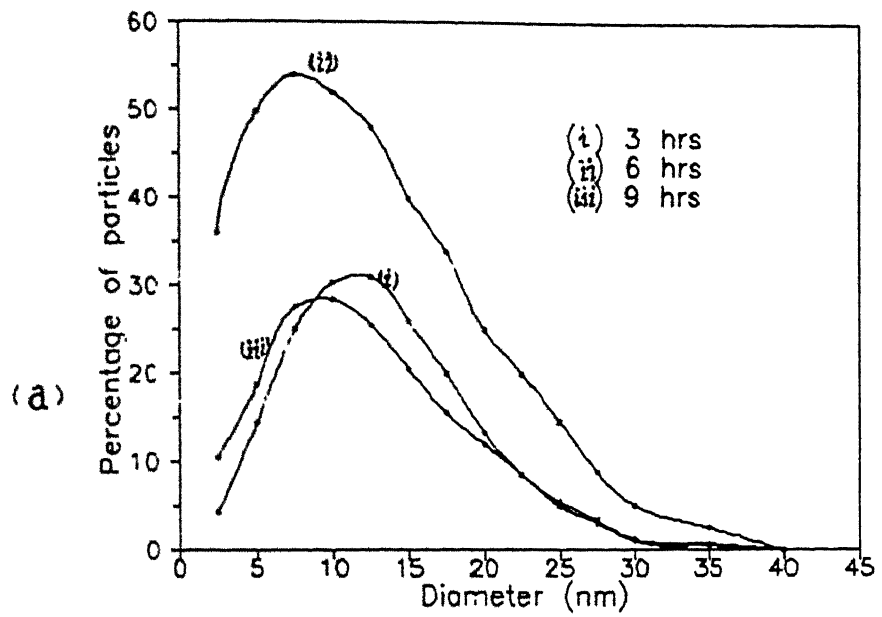
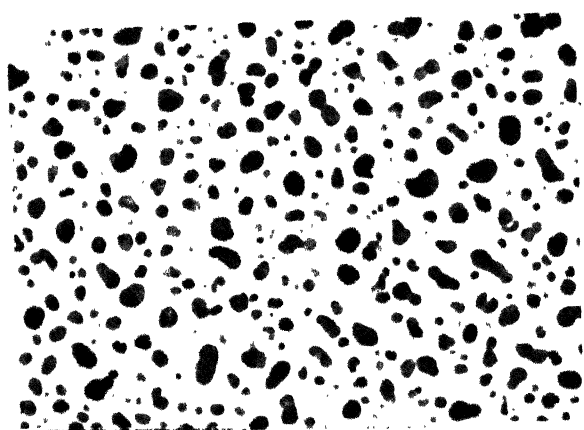
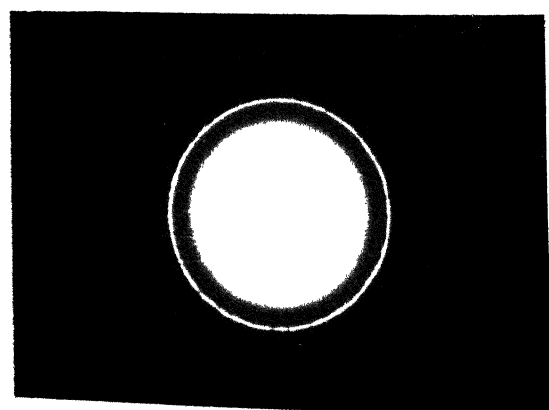


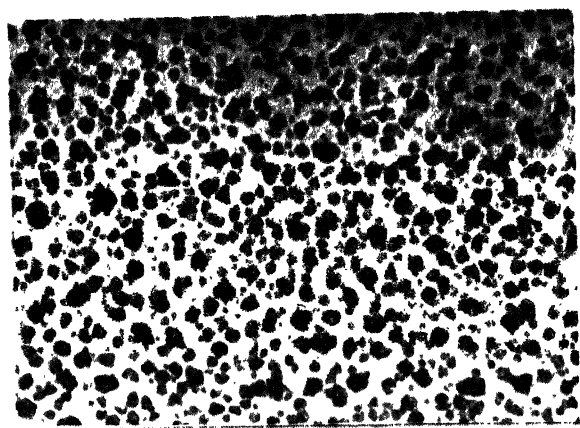
Fig.3.9: (a)Normal size distribution curves and (b)Cumulative percentage versus projected diameter plots of iron particles (mass thickness 1nm) in hydrogen atmosphere at 400C for (i)3h, (ii)6h and (iii)9h.



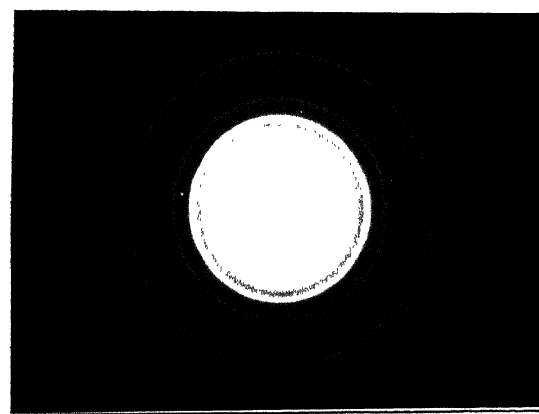
(a)



(c)



(b)



(d)

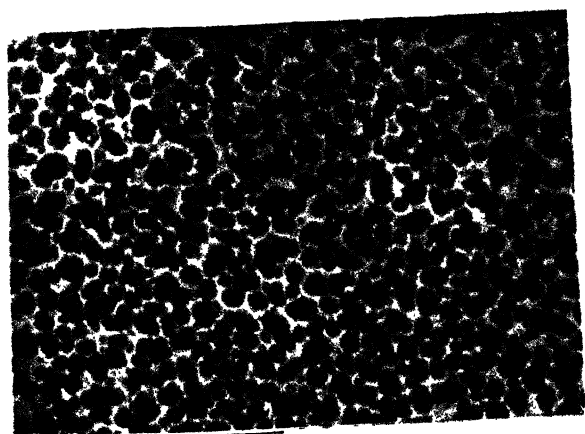
200nm  
|-----|

Fig.3.9: (a) and (b) Bright field transmission electron micrographs crystallites after heat treatment of iron particles (mass thickness 1.0nm) in hydrogen atmosphere at 500C for 2h and 7h, respectively; (c) and (d) electron diffraction pattern of regions shown in (a) and (b), respectively

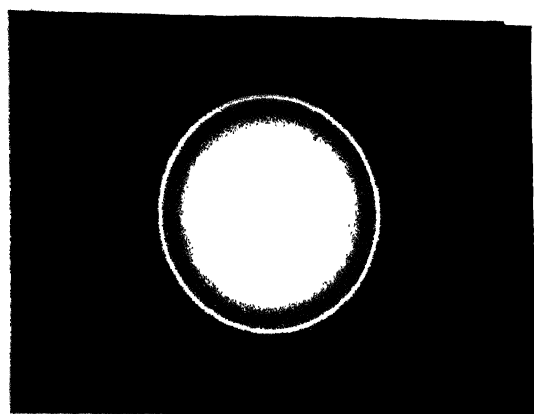
Table 3.5: Interplanar spacing and Miller indices of  $\text{FeAl}_2\text{O}_4$  crystallites formed, after heating  $\text{Fe}/\text{Al}_2\text{O}_3$  system of mass thickness 1.0nm, in hydrogen, at 500C for 7h.

Observed data		Miller Indices (hkl)	Known data [47]	
$d_{hkl} (\text{\AA}) \pm 0.04\text{\AA}$	Relative Intensity		$d_{hkl} (\text{\AA})$	Relative Intensity
-	-	111	4.709	3
2.94	S(+)	220	2.883	58
2.50	VS	311	2.4597	100
2.09	W	400	2.0382	17
-	-	331	1.8711	5
1.72	W	422	1.6649	16
1.61	S	511	1.5691	36
1.48	S	440	1.4414	42
-	-	620	1.2892	5
1.27	W(-)	533	1.2434	8
-	-	622	1.2293	3
1.21	VW	444	1.1769	2
-	-	551	1.1417	1
-	-	642	1.0897	5
1.09	W	731	1.0614	10

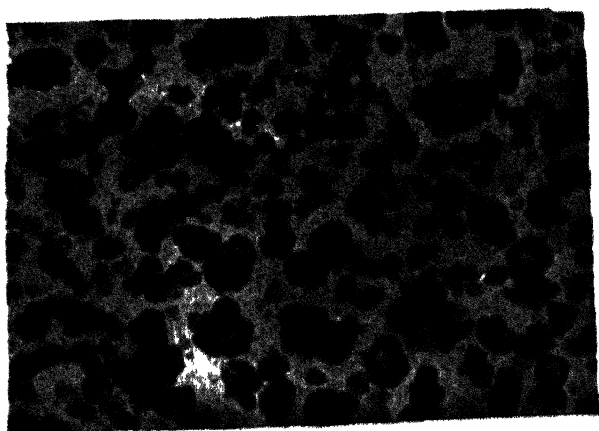
$$\text{Lattice parameter} = 8.36\text{\AA} \pm 0.04\text{\AA}$$



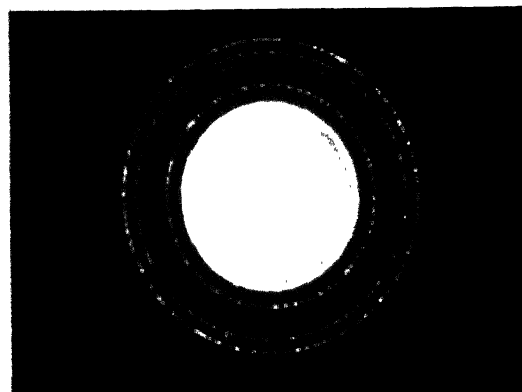
(a)



(c)



(b)

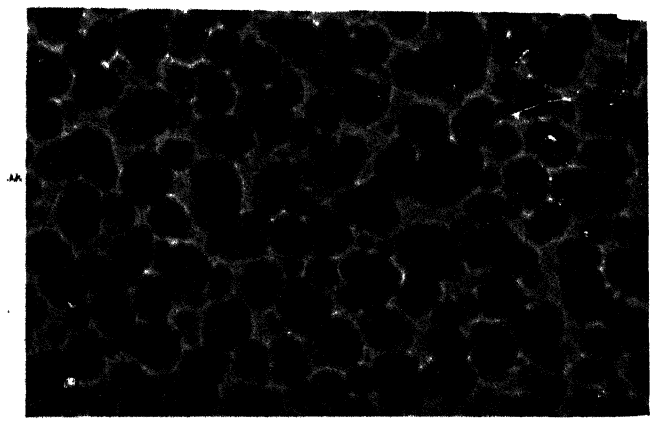


(d)

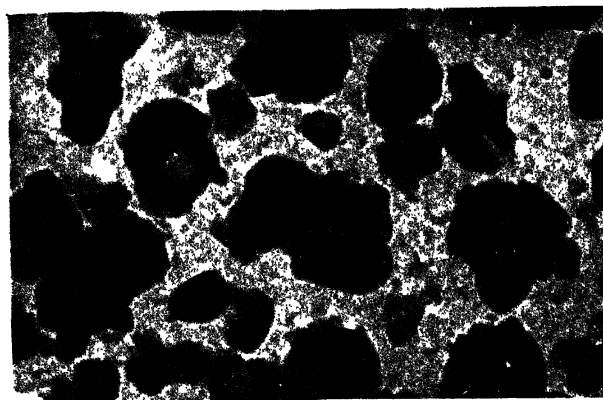
200nm

Fig.3.10: Bright field transmission electron micrographs of iron particles of mass thickness 1.5nm after heat treatment at (a) 400°C for 3h and (b) further treatment at 500°C for 5h; and (c) and (d) electron diffraction patterns of regions shown in (a) and (b) respectively.

microstructure together with diffraction pattern of 1.5 nm sample after heat treatment in hydrogen. It may be noted that the initially deposited iron film exhibit well separated platelet-type particles [Fig 3.2C] with particle size distribution parameters given in Table 3.2. But , on heating at 400°C for 3 hours, a distinct and curious morphology results viz., besides getting enlarged, an annular gap develops near the boundaries that separates the central region from the outer portion. This may be called as core-and-ring structure [Fig 3.10a]. A careful analysis of the corresponding selected area diffraction pattern [Fig 3.10c] reveals the presence of  $\text{Fe}_2\text{O}_3$ ,  $\text{FeAl}_2\text{O}_4$ , and Fe simultaneously. When this very sample was further heated in hydrogen at 500°C for 5 hours, very large crystallites emerged that exhibited torus shaped with an enclosed cavity [Fig 3.10b]. The diffraction pattern of such region [Fig 3.10d] corresponds to the cubic phase of the compound  $\text{FeAl}_2\text{O}_4$  with lattice parameter  $8.36 \pm 0.04 \text{ \AA}$ . Typical electron micrographs of (a) core-and-ring and (b) torus shaped particle are depicted in Fig 3.11 . The cavity inside the torus shaped particles was verified by recording two micrographs (i.e., stereo pairs ) of the same region at a tilt of 0 and 6° of the specimen and then viewing them together through a mirror stereoscope. Such an arrangement clearly depicts 3-dimensional feature of the region. The observation revealed the cavity formation with the outer mass above the surface of the substrate. Fig 3.12 shows the respective micrographs pasted in proper position side by side for the purpose of viewing through a stereoscope.



(a)



(b)

90nm

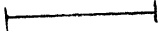
A horizontal scale bar with vertical end caps, indicating a length of 90nm.

Fig.3.11: Typical transmission electron micrographs of (a) core-and-ring and (b) torus shaped particles.



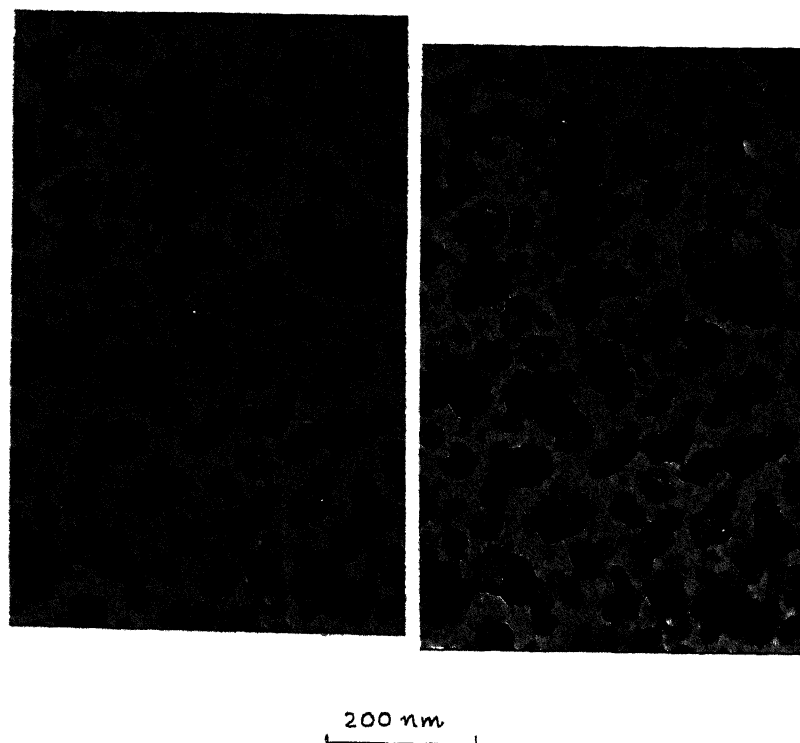


Fig.3.12: Transmission electron Micrographs of same region at a tilt  $0^\circ$  and  $6^\circ$  of the specimen exhibiting torus shaped crystallites for stereoscopic vision.

## (b) Effect of Oxygen

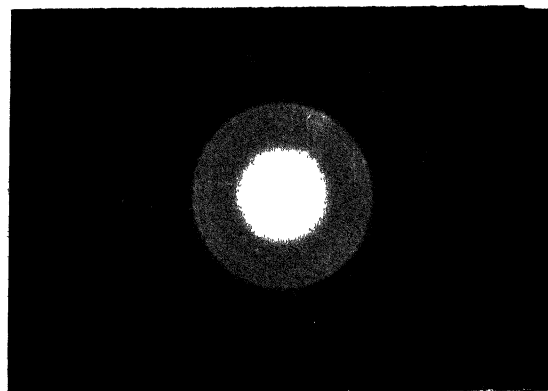
44

Iron particles of mass thickness 1nm dispersed over alumina at a substrate temperature of 500C were treated in oxygen atmosphere at 400C for 1, 2, and 4 hours. The microstructure invariably shows tremendous spreading of particles at their respective places, and many of them even touching each other. The crystallite morphology in all the above three cases is torus-type with large cavities. One representative microstructure and a typical selected area diffraction pattern are shown in Fig 3.13.<sup>(a,b)</sup> The analysis of diffraction pattern revealed the formation of  $\text{FeAl}_2\text{O}_4$  phase with lattice parameter  $8.26 \pm 0.04 \text{ \AA}$ . To check whether the reaction proceeds via formation of iron oxide, one sample was heated in oxygen at 300C for 45 minutes. The diffraction pattern again indicated the formation of  $\text{FeAl}_2\text{O}_4$  compound with none of oxide rings traced. However the diffraction rings were somewhat diffused in the latter case, displaying strains in the crystallites. Also, there appears to be substantial spreading of the crystallites over the substrate. The detailed evaluation of the micrographs revealed formation of a nearly continuous layer besides small torus shaped particles. Further, longer duration of heat treatment resulted in relatively sharp diffraction rings. From the above observation it may be concluded that oxygen greatly enhances the reaction of iron with alumina substrate.

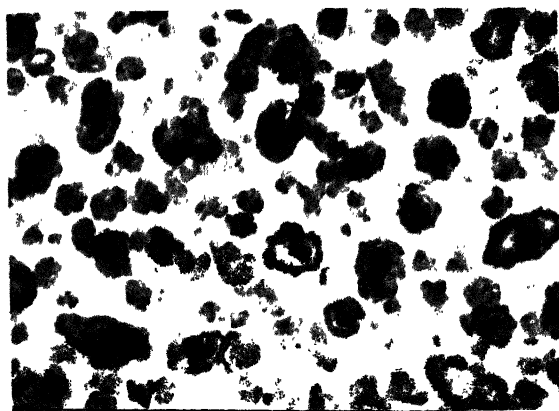
In yet another set, the previously two step heat treated (400C for 3 hours + 500C for 4 hours) sample of 1.5nm mass thickness in



(a)



(b)



(c)


200nm  


Fig.3.13:(a) Bright field transmission electron micrograph of crystallites after heat treatment of iron particles (1nm thickness) in oxygen atmosphere at 400°C for 4h, (b) electron diffraction pattern of region shown in (a) and (c) bright field transmission electron micrograph of crystallites after heating the same

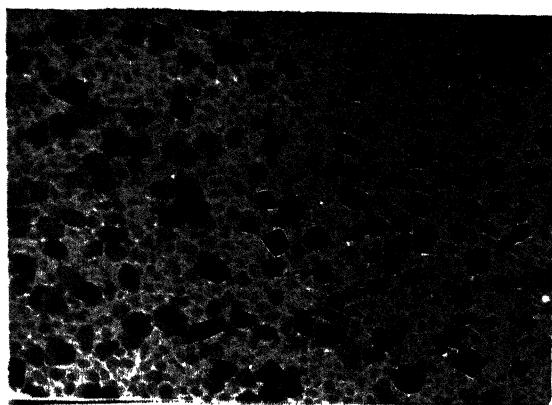
hydrogen was heated in oxygen for 2 hours at 500°C. This led to decrease in the crystallites size with many of them exhibiting core-and-ring structure<sup>[Fig 3.13c]</sup>. This suggests that the crystallites shape oscillate between the two types mentioned above, i.e., torus and core-and-ring structure. Sushumna and Ruckenstein [49] have also reported such instances of shape oscillations in particles during heat treatment at 400°C in locally supplied hydrogen. However, they pointed out that no such oscillations were seen when extra pure hydrogen was used. The particles in that case were claimed to be of iron only.

#### (c) Effect of vacuum

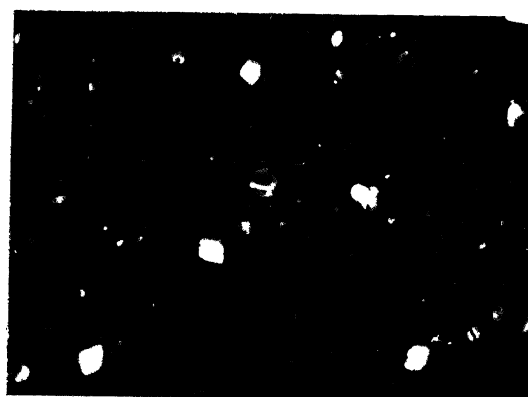
One sample of 0.8nm loading prepared at substrate temperature of 500°C was heated in vacuum of  $10^{-5}$  torr to study the coarsening phenomenon and/or accompanying chemical changes in iron. The sample heated at 500°C for 3 hours exhibits microstructure as shown in Fig 3.14a. A discontinuous film is formed by a host of fine grain crystallites. Also, a fairly good number of big particles, many of them exhibiting faceting character, are found scattered in the matrix. The corresponding electron diffraction pattern contains sharp rings [Fig 3.14c] and corresponds to  $\text{FeAl}_2\text{O}_4$  having a cubic structure with lattice parameter  $8.36 \pm 0.04 \text{ \AA}$ .

### 3.4 GENERAL DISCUSSION:

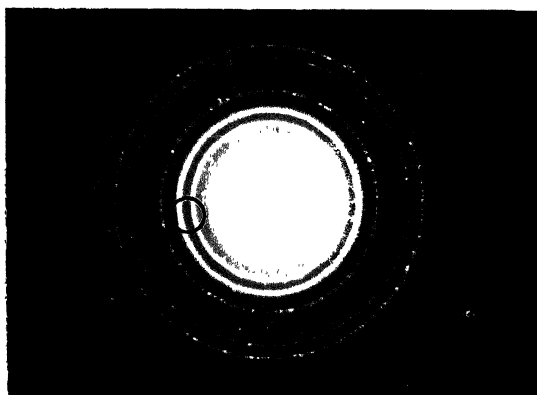
No exact comparative study is possible regarding the various particle size distribution parameters as the distribution itself



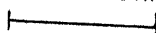
(a)



(b)



(c)

200nm  


3.14: (a) and (b) Bright field and corresponding dark field transmission electron micrograph after heat treatment of iron particles (mass thickness  $0.8\text{nm}$ ) in vacuum ( $<10^{-5}\text{torr}$ ) at  $500^\circ\text{C}$  for 3h; (c) electron micrograph of a single particle from a fraction of region shown in (a) with objective aperture used for

may sometimes vary with the local characteristics of the substrate even in the same specimen. Hence the size distribution of each loading should be treated independently as it is difficult to ensure the same physical nature in different substrates.

The fact that the size (average projected diameter) of iron particles becomes a bit smaller at substrate temperature of 500°C than those emerged at 450°C is at variance with the result of R. Palanisamy, V. Subramaniam and R. Saxena [15-18] on Ni, Au, and Pt and Pd, respectively. In all these cases, the particle size is reported to increase with substrate temperature. The present result when viewed in the light of these observations suggest that the size of the particles versus substrate temperature curve should pass through a minimum, provided all the other experimental conditions remain the same.

It is already established in the previous section that coarsening of particles occurs at elevated temperatures. Also, the extent of coarsening depends on the temperature and time both. Basically, two mechanisms are available to explain the growth of particles, namely (i) migration and coalescence, and (ii) Ostwald ripening. In the first, small metal particles resting on suitable support can grow by migration followed by interparticle collision and coalescence. Therefore, during the process of microstructure examination, one should encounter particles touching each other quite frequently. However, none of the micrographs presented in Figs 3.6, 3.9 and 3.10 matches with this description. The process of migration will further be hindered if the surface is rough and there exists strong interaction between metal particle and the support. Our observations at no stage have indicated possibility

of large scale movement of particles of even smallest possible size (i.e., 1nm). The main reason for not observing any migration over the substrate could possibly be due to strong interaction prevailing between the crystallites and the alumina support. This is more evident by the fact that even in vacuum of  $10^{-5}$  torr, iron particles react with alumina to form  $\text{FeAl}_2\text{O}_4$ . Also, the alumina support is amorphous in nature and so not at all smooth in the crystallographic sense. Therefore, it appears that temperature of 500°C used for heat treatment in the present work is not sufficient to cause particle migration. Sushumna and Ruckenstein [49, 50] have indeed observed particle migration above 700°C only.

In the second, movement of individual atoms take place from smaller particles to larger ones. In the process, some of the metal atoms dissociate from the particle to the surface of the support or go to the vapour phase temporarily. The strength of the bond between the atoms and the particle is determined by the size of the particle itself, being weaker for smaller particles. Consequently, the concentration of free atoms surrounding small particle becomes higher than near larger ones. The migration of atoms occur on the substrate due to their concentration gradient. Thus individual atoms appear to have migrated from smaller particles to regions surrounding the bigger particles. On capturing these excess atoms, bigger particles grow further while small ones decrease gradually in size and finally disappear. It implies that we should notice particles of small and big sizes at the same time during the intermediate coarsening stages atleast. Fig.3.6 and 3.9 indeed show this behaviour where small

and big particles appear simultaneously in vicinity of each other.

The interaction of crystallites with the support is still stronger in oxygen atmosphere as the reaction occurs even at 300°C and leads to the formation of  $\text{FeAl}_2\text{O}_4$  in just 45 minutes. This happens perhaps due to spreading of crystallites in oxygen atmosphere as greater surface area then comes in contact with the substrate than before. The behaviour of iron particles in oxygen can be understood in terms of changes in the interfacial tensions. The equilibrium condition is given by Young's equation [Fig1.3]

$$\gamma_{mg} \cos \theta = \gamma_{sg} - \gamma_{ms}$$

where  $\gamma_{mg}$ ,  $\gamma_{sg}$ , and  $\gamma_{ms}$  are crystallite-gas, substrate-gas and crystallite-substrate interfacial energies respectively, and  $\theta$  is the contact angle. When the metal particle is subjected to oxygen atmosphere or oxidized, its  $\gamma_{mg}$  changes and becomes smaller. Also the resulting oxide particles interact strongly with the oxide support (alumina in this case). As a consequence the interfacial energies  $\gamma_{ms}$  also decreases. The interfacial energy between the crystallite and the support is given by

$$\gamma_{ms} = \gamma_m + \gamma_s - U_{ms}$$

where  $U_{ms}$  is the interaction energy between crystallite and the support, and  $\gamma_m$  and  $\gamma_s$  are the surface tensions of the crystallite and support, respectively (when the gaseous phase is ignored). In



General  $\gamma_m \sim \gamma_{mg}$  and  $\gamma_s \sim \gamma_{sg}$ . If the two surfaces could be placed in contact without any intermolecular interaction the interfacial energy would be just equal to sum of their individual surface energies (i.e.  $\gamma_m + \gamma_s$ ). Since there are intermolecular interactions, the net interfacial energy is obtained by subtracting from the above sum the interaction energy  $U_{ms}$  of the two surfaces in contact. The decrease in  $\gamma_{mg}$  and  $\gamma_{ms}$  reduces the wetting angle  $\theta$ , and as a consequence the particles assume a smaller equilibrium angle on the substrate. The chemical interaction between the crystallite and the alumina leading to the compound formation  $FeAl_2O_4$  amounts to further increase in the value of  $U_{ms}$  making  $\gamma_{ms}$  still smaller. This reduction in the interfacial energy  $\gamma_{ms}$  and also a decrease in the value of  $\gamma_{mg}$ , caused by oxidation, lead to a rapid spreading of crystallite over the substrate.

Also, since  $FeAl_2O_4$  is formed in vacuum as well, two possible reasons for reaction to proceed could be (i) oxygen present in vacuum around  $10^{-5}$  torr is sufficient for supporting the reaction between iron crystallites and alumina to give  $FeAl_2O_4$  directly or through some iron oxide. This suggests that iron oxide and  $FeAl_2O_4$  should have formed during the creation of iron particles itself as the experimental conditions (vacuum  $\sim 10^{-5}$  torr) including the substrate temperature of  $500^\circ C$  were exactly the same. Also, iron being in atomic form during evaporation, could be highly reactive and therefore ~~it possibly~~ give oxide or  $FeAl_2O_4$  directly. But, the diffraction pattern of the dispersed particles shows no sign of any phase other than the pure iron. Hence, the oxygen present, if any, at  $10^{-5}$  torr does not possibly aid the reaction

process.(ii)strong bonding between iron and alumina and temperature of 500C are adequate to allow cause diffusion of atomic species through the interface and <sup>to eventually</sup> form  $\text{FeAl}_2\text{O}_4$ .

#### 4. CONCLUSIONS

1. Vacuum deposition of iron on alumina support films at substrate temperature around 500°C and working pressure of  $10^{-5}$  torr or less provides a way to obtain fine dispersion of well separated, platelet shaped particles. This method is unique in the sense that it envisages no prior heat treatment in any gaseous (especially hydrogen) atmosphere and therefore yields samples free from contaminations.
2. The extent of particle dispersion depends upon the substrate temperature and the amount of metal taken for evaporation e.g., for iron-alumina system, at a substrate temperature of 500°C, mass thickness in the range of 0.6-1.5 nm yields reasonable dispersion. The resulting samples were suitable for studying the behaviour of Fe/Al<sub>2</sub>O<sub>3</sub> system by transmission electron microscopy.
3. The average particle size depends strongly on the loading level (or mass thickness). The particle projected diameter decreases somewhat by raising the substrate temperature from 400 to 500°C for both 1.0nm and 1.5nm mass thicknesses.
4. Iron being the most electropositive of VIII group metals and so is highly reactive. Yet, the particles formed at substrate temperature in the range 200-500°C at a pressure of  $\sim 10^{-5}$  torr yields pure iron particles only. No evidence was found for any compound formation with the residual gases present during the deposition process.

5. There exist no evidence to support migration of particles on alumina support film in hydrogen atmosphere to permit their agglomeration, and hence coarsening by sintering mechanisms. On the other hand, the observations attribute coarsening to the Ostwald ripening, where large particle grow further at the expense of small ones by diffusion of species via the substrate from small to big crystallites.

6. In the oxidizing atmosphere, crystallites spread laterally at their respective places, assume torus shaped structure with large cavity and undergo chemical changes leading to formation of  $\text{FeAl}_2\text{O}_4$  and sometimes traces of  $\text{Fe}_2\text{O}_3$  as well.

7. The 1.5nm mass thickness iron film on heating in hydrogen at 400C for three hours leads to a mixture of Fe,  $\text{Fe}_2\text{O}_3$  and  $\text{FeAl}_2\text{O}_4$ . Moreover, the particles assumed core-and-ring structure. Further heating at 500C for 5hours in hydrogen results in big torus shaped particles displaying a cavity. However, the particles tend to assume back the core-and-ring structure after further heating in oxygen at 500C for 2hours.

8. In vacuum, neither torus nor core-and-ring type particles appear. Instead, the resulting microstructure shows a large number of small and irregular shaped particles in the background. Also, quite a few big crystallites emerge with sharp boundaries and exhibits faceting character.

9.  $\text{FeAl}_2\text{O}_4$  exhibits fcc structure with space group Fd3m and

lattice parameter varying in the range  $8.28 - 8.36 \pm 0.04 \text{ \AA}$  depending upon the atmosphere, e.g., the values of lattice parameter of  $\text{FeAl}_2\text{O}_4$  formed in hydrogen/vacuum and oxygen is  $8.36 \pm 0.04 \text{ \AA}$  and  $8.28 \pm 0.04 \text{ \AA}$  respectively. Thus, the lattice parameter of  $\text{FeAl}_2\text{O}_4$  is always found to be greater than the known bulk value of ( $8.1534 \text{ \AA}$ ).

## REFERENCES

1. J.E. Boudart, "Structure of metallic catalysts", Academic press, London, 1976.
2. M. Boudart, In: Proceedings of 6th International Congress on Catalysis, (Eds) J.C.Bond, P.B.Wells and F.C.Tompkins, Chemical Society London, 1977.
3. J.E. Boudart, H.Poppa, and M.Boudart., "Disproportionation of CO Supported Palladium on Small Particles of Silica", J. Catal. 41, (1976), 1-10.
4. J.Durrer, H.Popa, M.Dickinson and C.Park., "Decomposition of Ethylene on Small Palladium Particles", J. Vac. Sci. and Tech. A1 (1983), 1545-1548.
5. C.G.Granqvist and G.A.Nicholson., "Ultra Fine Chromium Particles for Photothermal Conversion of Solar Energy", J. Appl. Phys., 49, (1978), 3512-3520.
6. C.G.Granqvist, "Photothermal Conversion of Solar Energy by Gold Cermet Coatings J. Appl. Phys., 50,(1979),2916-2920.
7. T.H.James, "The Theory of the Photographic Process", 4th ed., McMillan, New York, 1977.
8. C.Hayashi, "Ultra-fine Particles", Physics Today 40,(1987), 44-51.
9. J.T.Waber, "Characterization and Behaviour of Materials with Submicron Dimensions", World Scientific, Singapore, 1985.
10. C.Hayashi, "Ultra-fine Particles", J. Vac. Sci. Tech. A5,(1987),1375-1384.
11. C.G.Granqvist and R.A.Buhrman, "Ultra-fine Metal Particles", J.Appl. Phys. 47, (1976), 2200-2218.

13. J.F.Hamilton and R.C.Baetzold, "Catalysis by Metal Clusters",  
Science. 205, (1979 ),1213-1220.
14. H.Poppa, "Model Studies in Catalysis with Ultra high vacuum  
Deposited Metal Particles and Clusters", Vacuum.  
(1984),1081-1095.
15. J.Kumar and R.Palanisamy, "Formation of Small Particles of  
Gold on Alumina Support Films and their Behaviour in Oxygen  
and Hydrogen Atmospheres", Appl. Surface Sc. 29, (1987),256-2
16. R.Saxena. "Electron Microscope Studies of Platinum and  
Palladium Catalysts on Carbon and Alumina Support Films",  
M.Tech. thesis, Indian Institute of Technology, Kanpur, (1983)
17. Anu gupta , "Electron Microscope Studies of Ultra fine Gold  
Particles Dispersed over Alumina Support Films", M. Tech.  
thesis, Indian Institute of Technology, Kanpur, (1986).
18. V.Subramanian "Dispersion of Nickel Particles on Alumina  
Support and their Behaviour in Oxygen and Hydrogen  
Atmospheres" M.Tech. Thesis, Indian Institute of Technology  
Kanpur,(1989).
- 19 S.A.Stevenson, J.A.Dumesic, R.T.K.Baker, and E.Ruckenstein,  
(eds), (1987), Chapter-7 and 8, "Metal Support Interactions  
in Catalysis,Sintering and Redispersion", Van Nostrand  
Reinhold, catalysis series New York.
20. M.Vannice. "Catalytic Synthesis of Hydrocarbons From H<sub>2</sub>/  
mixture Over The Group VIII Metals", J. Catal., 37, (1975),  
449-461 and 462-473.
21. V.D.Lee and V.Ponec, "On Some Problem of Selectivity in Syngas  
Reactions on Group VIII Metals", Cat. Rev. sci. - Eng., 29,  
(1987)183-218.

23. M.A.Vannice, "Titania-Supported Metals as CO Hydrogenation Catalysts", J. Catal. 74,(1982),199-202.
24. A.Tamiz and T.Yasukatsu, "Hydrogenation of Carbons Catalysed by Transition Metals", J. Catal., 27, (1972), 293-311.
25. Thomas and Lambert, "Characterisation of catalysts", John Wiley and sons, New York, 1980.
26. P.D.Cullity, "Elements of X-ray Diffraction", Second Edition, Addison Wesley, 1978.
27. H.P.Klug and Alexander, "X-ray Diffraction Procedure of Polycrystalline and Amorphous Materials", John Wiley, 1974.
28. J.P.Huffman and H.H.Podgurski, "Electron Re-emission Mossbauer Study of Oxidation of Metallic Iron in Oxygen", Oxidation of Metals, 10, (1976), 377-401.
29. G.E.Raupp and W.N.Delgass, "Mossbauer Investigation of Support Fe and Fe-Ni Catalysts", J. Catal., 58, (1979) 337-347;348-368.
30. Z.Paal and P.G.Menon, "Hydrogen Effect in Metal Catalysts", Cat. Rev.-Sci. Eng., 25(2), (1983), 229-324.
31. I.W.Bassi, F.W.Lytle and G.Parravano, "Study of Chemical Reactivity of Supported Gold by X-ray Absorption Fine Structure Spectroscopy", J. Catal., 42, (1976), 139-147.
32. R.A.Young, "Third International Conference on Small Angle Scattering, Grenoble", J. Appl. Cryst., 7, (1973), 95-101.
33. V.Gerold, "Small Angle Scattering Application to Material Science", J. Appl. Cryst., 11, (1978), 376-404.
34. M.J.Yacman, "Characterisation of Supported Catalysts by Transmission Electron Microscopy", J. Appl. Catal. 13, (1984) 1-25.



34. P.L.Matyti, L.H.Schwartz and J.B.Bowt, "Particle Size, Particle Size Distribution and Related Measurements of Supported Metal Catalysts", Catalytic Rev. Sci. and Engg. 29(1), (1987), 41-99.
35. N.M.Pillar and J.Nutting, "Solid-Solid Interfacial Energy Determination in Metal-Ceramics Systems", Phil. Mag., 16, (1987), 181-188.
36. T.Huizinga, J.V.Grondelle and R.Prins, "Temperature Programmed Reduction Study of Platinum on Alumina and Titania", Appl. Catal., 13, (1984), 199-213.
37. J.S.Smith and M.A.Vannice, "Characterisation of Ni/TiO<sub>2</sub> Catalyst by TEM, X-Ray Diffraction and Chemisorption Techniques", 68, (1981), 270-285..
38. P.J.Tatarchuk, J.A.Dumesic, "Physical Characterisation of Fe/TiO<sub>2</sub> Model Supported Catalysts", J. Catal., 70, (1981), (323-334, 335-346, and 308-322).
39. L.Young, "Anodic Oxide Films", Academic press, New york, 1961.
40. G.Hass, "Preparation of Hard Oxide Films with Precisely Controlled Thickness on Evaporated Aluminium Mirrors", J. Opt. Soc. of America, 39, (1949), 532-544.
41. P.B.Hirsch, A.Howie, R.B.Nicholson, W.Pashley and W.J.Whelan, "Electron Microscopy of Thin Crystals", Butterworth, London, 1967.
42. R.Bares and V.B.Cosslett, "Advances in Optical and Electron Microscopy", p33, Vol.3, Academic press, (1969).
43. R.R.Irani and C.F.Callis, "Particle size: Measurement, Interpretation and Application", John Wiley, New York, 1965.

44. R.T.Dehoft and F.N.Rhines, "Quantitative Microscopy" Mc Graw Hill, New York, 1968.
45. Kiyosi Ito, Encyclopedic dictionary of mathematics, Second edition, Vol. III (o-z), MIT press, Massachussets, 1986.
46. Powder Diffraction File No. 8-696.
47. Powder Diffraction File No. 34-192.
48. I.Sushumna and E.Ruckenstein, "Role of Physical and Chemical Interactions in the Behaviour of Supported Metal Catalysts: Iron on Alumina- A Case Study", J. Catal., 94, (1985), 239-288.
49. I.Sushumna and E.Ruckenstein, "Oscillations in Crystallite shape during Heating in Hydrogen of Model Iron/Alumina Catalysts", J. Catal. 90, (1984), 241-255.
50. E.Ruckenstein and I.sushumna, "Multilayer Surface Films Coexisting with Crystallites in Model Iron/Alumina Catalysts", J. Catal., 97, (1986), 1-24.



**11771**

TH  
530.41  
R137c

**1A**

Date Slip **117718**

This book is to be returned on the  
date last stamped.

This image shows a blank sheet of white paper with horizontal ruling lines. A single vertical line runs down the center of the page, creating two equal-width columns. The horizontal lines are evenly spaced and extend across the entire width of the paper, including both columns. There are approximately 20 horizontal lines visible. The paper appears to be a standard notebook or ledger page.

MS-1994-M-RAN-ELE